

DESIGN AND CONSTRUCTION OF A HIGH PRESSURE SYSTEM FOR
EVALUATING MULTIPHASE TWIN-SCREW PUMPS

A Thesis

by

THEODORE ISAAC HATCH

Submitted to the Office of Graduate and Professional Studies of
Texas A&M University
in partial fulfillment of the requirements for the degree of

MASTER OF SCIENCE

Chair of Committee,	Gerald Morrison
Committee Members,	Andrew Duggleby
	Robert Randall
Head of Department,	Andreas Polycarpou

December 2013

Major Subject: Mechanical Engineering

Copyright 2013 Theodore Isaac Hatch

ABSTRACT

Twin-screw pumps are currently sold by manufacturers without adequate data predicting the pump behavior when pumping multiphase mixtures. In light of the fact that pump behavior is known to change significantly under these conditions, a new closed-loop test facility has been designed and constructed to allow for testing of twin-screw pumps at high gas volume fractions. With minimal modification, the test facility can accommodate high pressure flows and oil-based liquids for testing.

The closed-loop test facility supplies air and water to the inlet of an MR-200 twin-screw pump of which the performance characteristics are desired. The flow of air and water can be regulated to give the desired inlet pressure, outlet pressure, and gas volume fraction. The resulting mixture is driven to the test pump by its inlet suction. It then passes through the pump to a gravity separator, where it is separated into discrete liquid and gas phases. Inlet pressures up to seventy-five psig can be used, and with minimal modification, up to three-hundred psig. Total flow rates of up to six-hundred-fifty gallons per minute can be accommodated. A two-hundred horsepower electric motor provides the mechanical power for the pump.

The test facility includes instrumentation and data acquisition equipment to monitor the pressures and temperatures at various points in the flow loop, as well as the flow rate and motor voltage of the pump. The closed-loop facility is validated by comparing the

volumetric efficiency, mechanical efficiency, and pump effectiveness results to a previous open-loop facility that was also used to test the same twin-screw pump. Suggestions are given to replace an air valve to allow for more precise control of the air supply and to add a pulsation dampener that will moderate pressure oscillations. High pressure piping and tubing must be added for testing at higher inlet pressures.

DEDICATION

I dedicate this work to God, my wife, and my son, for their constant love, patience, and support through the good and bad times. I also dedicate this work to my mother and father, who instilled in me a love of learning, questioning, and finding answers.

ACKNOWLEDGEMENTS

I would like to thank my committee chair, Dr. Morrison, with the most sincere appreciation for his continued support, guidance, and intellectual assistance. I would also like to thank my committee members, Dr. Duggleby and Dr. Randall, for serving on my committee and for their support.

I would like to thank Abhay, Joey, Klayton, Sahand, Muhammet, Andrew, and Chase for helping with construction of the test facility. I would also like to thank Sahand for his vast expertise in data acquisition. Thanks to Sujan, Scott, Daniel Z., and Daniel S., and everyone else for always being available whenever I had questions, and for making my time at the Turbomachinery Laboratory a very enjoyable experience.

Lastly, thanks to my wife, for her extreme sacrifice and patience in helping me to finish graduate school, without whom I would be lost.

NOMENCLATURE

GVF	Gas volume fraction
η_V	Volumetric efficiency
η_M	Mechanical efficiency
η_{eff}	Pump effectiveness
P_p	Power imparted by pump to fluid
P_e	Electric power
P_h	Hydraulic power
P_{iso}	Isothermal power
P_{poly}	Polytropic power
p	Pressure
Δp	Pump differential pressure
Q_a	Actual total flow rate through pump
Q_{th}	Theoretical total flow rate through pump
Q_{liq}	Liquid volumetric flow rate
Q_{gas}	Gas volumetric flow rate
T	Temperature
V_{ml}	Motor load voltage

TABLE OF CONTENTS

	Page
ABSTRACT	ii
DEDICATION	iv
ACKNOWLEDGEMENTS	v
NOMENCLATURE.....	vi
TABLE OF CONTENTS	vii
LIST OF FIGURES.....	ix
LIST OF TABLES	xii
1 INTRODUCTION	1
1.1 Background	1
1.2 Objective	3
2 LITERATURE REVIEW.....	4
2.1 Twin-Screw Pumps	4
2.2 Pump Performance Metrics.....	5
3 DESIGN OF EXPERIMENTAL FACILITY	7
3.1 Overview of Design	7
3.2 Separator.....	12
3.3 Twin-Screw Pump.....	16
3.4 Circulation Pump	18
3.5 Piping and Filtering.....	20
3.6 Heat Exchangers.....	24
3.7 Flow Control Valves	27
3.8 Flow Meters	29
3.9 Instrumentation and Data Acquisition.....	31
3.10 Electrical Power System.....	42
3.11 Method of Operation	43
4 CONSTRUCTION AND ASSEMBLY	46

4.1	Separator.....	46
4.2	Piping and Control Valves	46
4.3	Heat Exchangers and Circulation Pump.....	47
5	RESULTS.....	52
5.1	Closed-loop Results	52
5.2	Comparison with Previous Facility	64
6	CONCLUSIONS	76
6.1	Conclusions	76
6.2	Recommendations	76
	REFERENCES.....	78
	APPENDIX A UNCERTAINTY ANALYSIS	79

LIST OF FIGURES

	Page
Figure 1: Diagram of twin-screw pump [3]	2
Figure 2: Diagram of flow loop.....	9
Figure 3: Gravity separator	13
Figure 4: Pipe reducer	14
Figure 5: Water level indicator tube.....	15
Figure 6: Colfax MR-200 twin-screw pump	16
Figure 7: Rotameter flow control valves for seal flush.....	17
Figure 8: Circulation pump	19
Figure 9: Air pressure regulator	21
Figure 10: Main water filter	22
Figure 11: Heat exchangers and support structure	25
Figure 12: Heat exchangers and support structure being lifted into place	26
Figure 13: Water flow control valves.....	27
Figure 14: Air control valve	28
Figure 15: Outlet control valve	29
Figure 16: Rotary flow indicator.....	31
Figure 17: Pressure transducer at pump outlet	32
Figure 18: Thermocouple	34
Figure 19: Omega iServer microservers.....	35

Figure 20: LabVIEW PID control	37
Figure 21: LabVIEW valve control.....	38
Figure 22: LabVIEW GVF calculations.....	39
Figure 23: LabVIEW warning lights.....	40
Figure 24: Left side of front panel of LabVIEW program.....	41
Figure 25: Right side of front panel of LabVIEW program.....	41
Figure 26: Variable frequency drive	42
Figure 27: Compressor removal from HVAC unit.....	48
Figure 28: Installation of heat exchanger support structure	49
Figure 29: Circuit breaker for heat exchanger fans.....	50
Figure 30: Circuit breaker and motor starter for circulation pump	51
Figure 31: Volumetric efficiency at 15 psi inlet pressure and 900 RPM	55
Figure 32: Volumetric efficiency at 50 psi inlet pressure and 900 RPM	56
Figure 33: Mechanical efficiency at 15 psi inlet pressure and 900 RPM	57
Figure 34: Mechanical efficiency at 50 psi inlet pressure and 900 RPM	58
Figure 35: Pump effectiveness at 15 psi inlet pressure and 900 RPM	60
Figure 36: Logarithmic increase in power in isothermal gas compression.....	61
Figure 37: Pump effectiveness at 50 psi inlet pressure and 900 RPM	63
Figure 38: Volumetric efficiency in new facility (15 psi inlet, 900 RPM, 100°F)	65
Figure 39: Volumetric efficiency in previous facility (15 psi inlet, 900 RPM, 75°F)	65
Figure 40: Volumetric efficiency in new facility (50 psi inlet, 900 RPM, 105°F)	67
Figure 41: Volumetric efficiency in previous facility (50 psi inlet, 900 RPM, 75°F)	67

Figure 42: Mechanical efficiency in new facility (15 psi inlet, 900 RPM, 100°F).....	69
Figure 43: Mechanical efficiency in previous facility (15 psi inlet, 900 RPM, 75°F).....	69
Figure 44: Mechanical efficiency in new facility (50 psi inlet, 900 RPM, 105°F).....	71
Figure 45: Mechanical efficiency in previous facility (50 psi inlet, 900 RPM, 75°F).....	71
Figure 46: Pump effectiveness in new facility (15 psi inlet, 900 RPM, 100°F)	73
Figure 47: Pump effectiveness in previous facility (15 psi inlet, 900 RPM, 75°F)	73
Figure 48: Pump effectiveness in new facility (50 psi inlet, 900 RPM, 105°F)	74
Figure 49: Pump effectiveness in previous facility (50 psi inlet, 900 RPM, 75°F)	74

LIST OF TABLES

	Page
Table 1: Test matrix for pump evaluation	11
Table 2: Water flow meters	30
Table 3: Air flow meter	30
Table 4: Pressure transducer locations	33
Table 5: Thermocouple specifications	34
Table 6: Data acquisition modules	36
Table 7: Liquid flow rate measurement equipment uncertainty	79
Table 8: Water flow meter uncertainties	81
Table 9: Air flow rate measurement equipment uncertainties	81
Table 10: Air flow meter uncertainties	82
Table 11: Air flow rate uncertainty at pump inlet.....	84
Table 12: GVF uncertainty.....	85
Table 13: Volumetric efficiency uncertainty	86
Table 14: Mechanical efficiency uncertainty	87
Table 15: Pump effectiveness uncertainty	88

1 INTRODUCTION

1.1 Background

Twin-screw pumps are used in the oil industry to pump multiphase flows in a single pipeline where a separator, compressor, and two pipelines would otherwise be required. The ability to use existing single pipelines to pump multiphase mixtures to a processing facility instead of separating natural gas for flaring or transport can reduce capital costs and be economically advantageous.[1] However, care must be taken to choose the correct pump for the correct application. Although twin-screw pumps are marketed for use in multiphase flows, current pump performance data from manufacturers focuses on the behavior while pumping a single-phase liquid. As such, the performance data for multiphase flows is lacking, and requires further investigation.

The field of multiphase pumping is composed of positive displacement pumps and rotodynamic pumps. Rotodynamic or centrifugal pumps operate using centrifugal force to accelerate and compress fluid. Rotodynamic pumps often contain multiple impeller stages to gradually increase the pressure of a working fluid. Centrifugal pumps have historically been ineffective at pumping multiphase flows because the impeller geometry must be tuned to be efficient in narrow Gas Volume Fraction (GVF) ranges. New designs of centrifugal pumps such as the Multi-Vane Pump (MVP) have the ability to operate in larger gas volume ranges. However, outside the designed GVF operating range, centrifugal pumps are not effective for pumping multiphase flows.[2]

Positive displacement pumps do not suffer from the same narrow GVF range drawbacks that centrifugal pumps experience, and many can operate at 0.0 - 1.0 GVF. Positive displacement pumps work by sealing a volume of fluid and forcing it from the inlet to the outlet by means of screws, pistons, or diaphragms.

One type of positive displacement pump, the twin-screw pump, operates by using two counter-rotating screws within a casing to trap volumes of fluid and pass them from inlet to outlet, similar in concept to an Archimedes Screw. These pumps often take advantage of mirroring the screws over the outlet to reduce the net thrust on the bearings to zero, as shown in Figure 1.

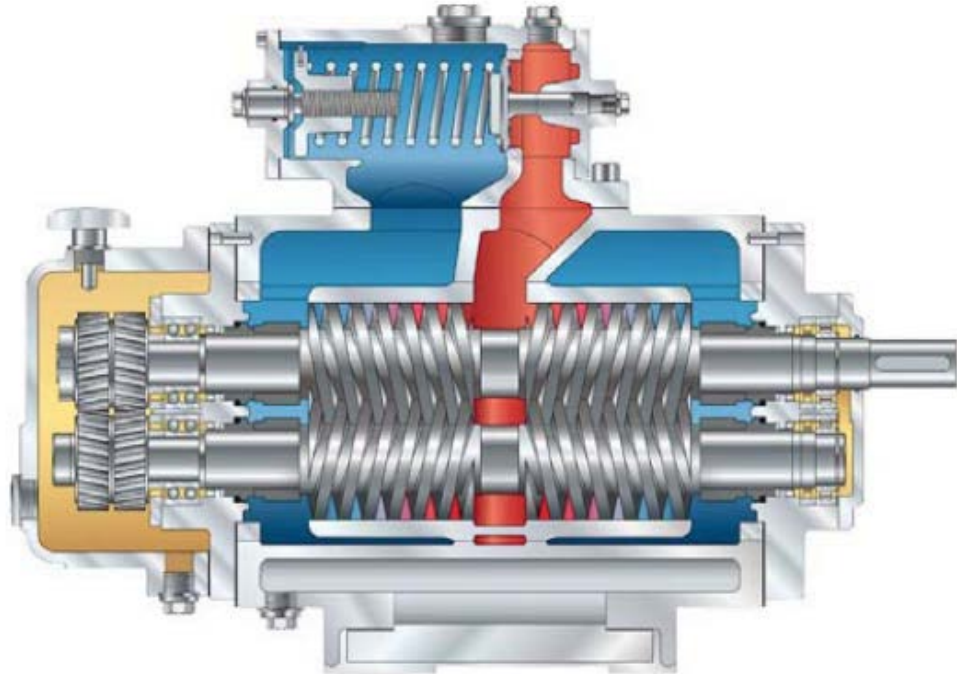


Figure 1: Diagram of twin-screw pump [3]

Twin screw pumps can theoretically operate at GVF's ranging from 0.0 - 1.0.[4]

However, due to friction of the screws in the casing there should be some small amount of recirculating fluid to lubricate the screws as well as seal the clearances of the screws to reduce the internal leakage of gasses from the high to low pressure regions.

Minimizing the leakage flow rate is of particular interest, with specific research being conducted investigating the effects of viscosity, temperature of the liquid, as well as the pressure differential across the screws.[5]

The multiphase flows that oil pumps experience are composed of a variety of gas and liquid phase hydrocarbons. Testing facilities often use water and air instead of hydrocarbons for ease of construction and maintenance of the testing equipment.[4]

1.2 Objective

The objective of this study was to design and construct a two-phase flow system that had a smaller footprint than the existing system, and had the capability to operate at higher inlet pressures. The system had to incorporate the ability to use a variety of testing fluids, including water-air mixtures as well as oil-nitrogen mixtures. The system had to control and vary the GVF, flow rate, and inlet and exit pressures to a pump.

Once constructed, the experimental facility was used to evaluate the operational characteristics of a twin-screw pump. Data from the new facility was compared to data from the previous facility to validate the efficacy of the new facility.

2 LITERATURE REVIEW

2.1 Twin-Screw Pumps

Performance testing and characterization of twin-screw pumps is not a new field. However, the capabilities of twin-screw pumps are increasingly being studied, due to the inherent ability to pump large gas volume fractions and the subsequent potential cost savings.

The basic concept of a screw pump dates back to the Archimedes Screw, which uses a single inclined screw in a casing to move liquids. Its invention is attributed to Archimedes of Syracuse around 200-300 B.C, and in the subsequent time the use of screw pumps has expanded to provide for basic water transmission and agricultural needs throughout the world. Twin-screw pumps have become increasingly utilized in the oil and gas industry in the last thirty years due to the potential for cost savings in using a twin-screw design. [2] The main advantage is that twin-screw pumps are able to pump gas volume fractions ranging from 0%-100% in some cases.[1] Using a twin-screw pump and a single pipeline instead of a traditional separator, pump, compressor, and twin pipelines reduces the initial capital cost of the equipment as well as the operating costs.

2.2 Pump Performance Metrics

Characteristic parameters of interest include the volumetric efficiency of the pump, the mechanical efficiency of the pump, and the effectiveness of the pump. The volumetric efficiency of the pump shown in Equation 1 is defined as the ratio of the actual flow rate to the theoretical flow rate, where the theoretical flow rate is specified by the screw geometry.

$$\eta_V = \frac{Q_a}{Q_{th}} \quad (1)$$

The mechanical efficiency of the pump is calculated as the ratio of the net power imparted to the fluid to the electric power supplied to the pump, as shown in Equation 2.

$$\eta_M = \frac{P_p}{P_e} \quad (2)$$

The net power at low GVF is calculated applying the assumption that the process is isothermal. It has been experimentally determined that the change in temperature of the water through the pump is negligible due to working liquid's high specific heat for low GVF. This net power is given in Equation 3.

$$P_{iso} = Q_{liq} \Delta p + p_{in} Q_{gas} \ln \left(\frac{p_{out}}{p_{in}} \right) \quad (3)$$

The net power for high GVF must account for the increase in temperature of the multiphase fluid. The net power in this case is calculated under the assumption that the process is polytropic, given by Equation 4.

$$P_{poly} = Q_{liq}\Delta p + \frac{n}{n-1}p_{in}Q_{gas} \left[\left(\frac{p_{out}}{p_{in}} \right)^{\frac{n-1}{n}} - 1 \right] \quad (4)$$

The hydraulic power is calculated as the sum of the liquid and gas volumetric flow rates multiplied by the change in pressure across the pump, as shown in Equation 5. This quantity represents the power that would be imparted to the flow if it were incompressible. This assumption is invalid for multiphase flow.

$$P_h = (Q_{liq} + Q_{gas})\Delta p \quad (5)$$

The pump effectiveness is calculated as the ratio of the net power imparted to the compressible multiphase fluid (under the isothermal or polytropic assumption from Equations 3 and 4) and the power added to an incompressible fluid (Equation 5). This parameter characterizes the effectiveness of the pump at compressing multiphase mixtures compared to fully incompressible liquid. The effectiveness is given by Equation 6.

$$\eta_{eff} = \frac{P_p}{P_h} \quad (6)$$

The metrics presented above will be used to evaluate the pump's performance.

3 DESIGN OF EXPERIMENTAL FACILITY

3.1 Overview of Design

The previous experimental system used large-volume air compressors to supply the gas and used centrifugal water pumps attached to a 5,000 gallon tank to supply water, which were then mixed to supply the multiphase pump with inlet pressures up to 100psig. A pressurized closed-loop system incorporating a 300 gallon gravity separator and an auxiliary cooling system was used to replace the previous system. The use of a smaller reservoir decreased the required footprint for the testing system by 56%. The pressurized system eliminated the need for large volume air compressors and boost pumps to provide the gas/liquid inlet supply. With replacement piping the system can also be used to test pumps at higher inlet pressure than the previous system without the need for boost pumps and pressure regulators. Water-air and oil-nitrogen mixtures can be used due to the sealed nature of the closed-loop system over the previous system where the reservoir was open to the atmosphere. The relatively small size of the separator reservoir will reduce the initial material cost of the oil-based testing fluid and will reduce the environmental impact in the event of a leak, should such a fluid be required at a future date. The new system was evaluated using air and water mixtures.

The pump chosen to evaluate this flow system is a Colfax MR-200 Twin-Screw pump. The separated liquid is recirculated to the pump inlet through a 141 micron water filter to protect the pump and instrumentation from any particles of corrosion that are dislodged

in the separator. The liquid passes through a parallel bank of three electro-pneumatic control valves to set the inlet liquid flow rate to the pump. The valves control the flow through three parallel turbine flow meters which record the liquid flow rate with capacities ranging from 0.75 – 225 GPM. The liquid then enters the pump inlet.

The gas separated from the two-phase mixture exits the gravity separator at the top, where it passes through two air filters in parallel to remove any droplets of water still contained in the air. The air then passes through a single gas turbine meter, where the pressure and temperature are recorded via a thermocouple and pressure transducer to obtain the mass flow rate of the gas. The air is directed to an electro-pneumatic control valve to set the inlet gas flow rate to the pump. The gas then enters the pump inlet.

The two phases enter the pump inlet and are pressurized through the rotating action of the screws. The flow reaches the outlet, where the outlet pressure is set by a single electro-pneumatic control valve. The flow then enters the separator where it is again separated into two distinct phases, and begins the cycle again.

The volumetric flow rate capacity of this particular twin screw pump is 633 GPM while the capacity of the separator tank is 300 gallons. This means that without any cooling loop, the operating temperature of the closed-loop system would increase rapidly. Thus, an auxiliary cooling loop was utilized to suppress the transient temperature effects of continuously recirculating the same liquid and gas. This cooling loop utilized two off-

the-shelf home HVAC condensers. The refrigerant and compressors were removed to leave only the copper tubing, coils, and fan. Liquid is taken from the separator with a 15 hp centrifugal circulation pump and flows through the two heat exchangers in parallel before it is returned to the separator. The auxiliary cooling loop is protected by an 800 micron y-strainer to remove any large particles which might cause blockages in the small copper tubing. A rotary flow sight is used to ensure flow through the heat exchangers. The circulation pump is also used to supply the 16 GPM of seal flush that the twin-screw pump requires for cooling and lubrication. The full air and water flow path of the system is shown in Figure 2.

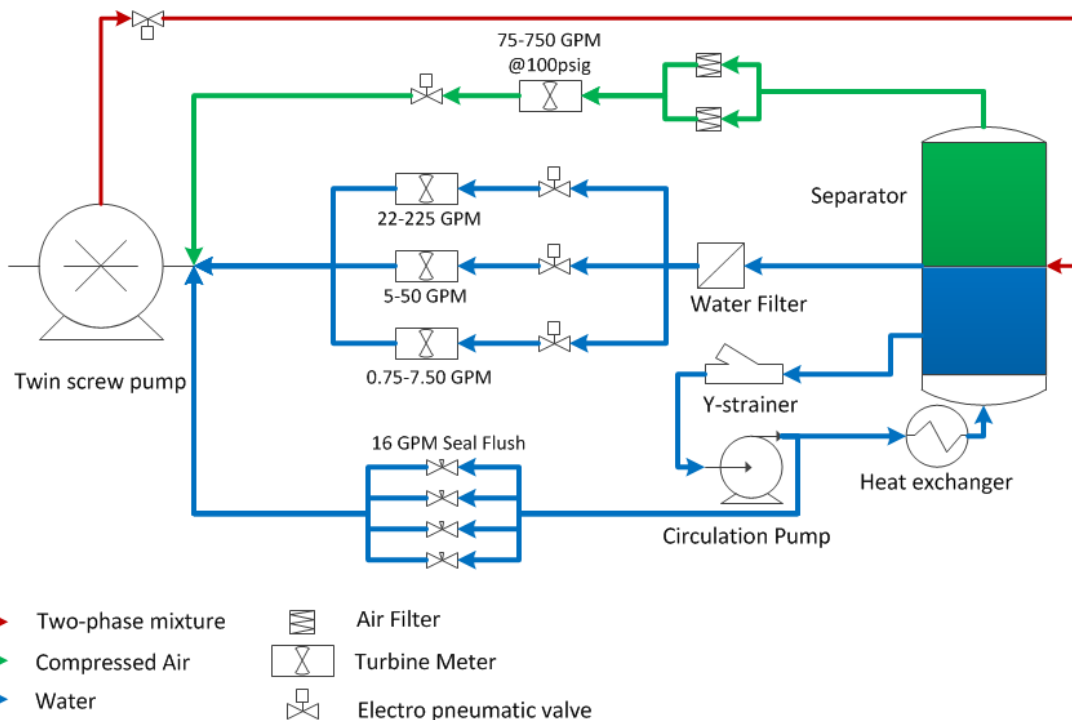


Figure 2: Diagram of flow loop

Due to financial constraints, this study utilizes schedule 80 chlorinated polyvinyl chloride (CPVC) piping, which can withstand ultraviolet radiation from the sun. However, this piping is limited in pressure by the weakest point in the system, which is a section of 4" CPVC pipe at the outlet of the pump. The limiting pressure is 320 psi at 73°F at this point. The operating temperature of this system is proposed to be up to 140°F in some situations, requiring a 50% pressure derate due to temperature. [6] Therefore the operating pressure must not exceed 160 psi. To provide a factor of safety and reduce the chance of even intermittently over pressurizing the flow system, a 125 psi relief valve was chosen for the separator which will vent to atmosphere when the pressure is exceeded. To reach higher operating pressures in the future, the separator, sensors, transducers, and other instrumentation has been chosen to withstand up to 300 psi. The heat exchanger hoses and coils can also withstand up to 300 psi. When funds are available, only the piping, manual ball valves, and minor fittings must be replaced to reach higher pressures.

All electro-pneumatic valves are electronically controlled by a PID program written in LabVIEW. Utilizing a PID controller increased the safety of the system by responding very quickly to changes in pressure, and reduced the chances of over pressurizing any one segment of piping. The program included the ability for the user to set the inlet and exit pressures, as well as the GVF.

Pressure and temperature data is gathered at each flow meter to allow calculation of mass flow rate from the measured volumetric flow rate. The pressure of the fluid is also measured after each valve at the inlet to account for changes in density due to change in pressure. The GVF is calculated based upon the ratio of the volumetric flow rates of air and water at the pump inlet.

The pump was tested under several different conditions by varying the GVF and inlet and outlet pressures of the pump. The instrumentation is verified by running the pump under the same conditions under which it has been previously tested with the old flow loop. The results are compared. The experimentation of the pump was then further expanded to include a higher inlet pressure at a range of GVF, as shown in Table 1.

Table 1: Test matrix for pump evaluation

Inlet Pressure [psig]	GVF	Differential Pressure [psig]
15	0.65	50-300
	0.80	
	0.90	
	0.92	
50	0.65	50-300
	0.80	
	0.90	
	0.92	

3.2 Separator

The separator chosen for the experimental facility is a 300 gallon gravity gas diverter, shown in Figure 3, and was manufactured by the Baker Tank Company. The separator was previously stored outside and was exposed to the elements. The inside of the separator had prevalent surface corrosion and the drain valve was rusted open. The flange faces that were exposed to the elements had significant surface rust that would impede proper gasket contact.

The separator has a 30" x 72" cylindrical vessel that can withstand pressures up to 737 psi at 100°F. The separator operates by providing a sealed chamber for the two-phase outlet mixture from the pump to enter. Once inside the separator, the flow passes through simple vanes that redirect the flow around the contour of the separator. Avoiding direct impingement against the separator wall in this manner reduces the aeration of liquid water into the air. Due to gravitational forces, the water falls to the bottom of the separator forcing the air upwards.



Figure 3: Gravity separator

Eight flanged connections of varying sizes and three pipe thread connections of varying sizes provide the inlet and outlet connections. The largest flanged connections were chosen for water outlet and two-phase inlet to the separator. Pipe spool reducers (one shown in Figure 4) were manufactured to reduce the pipe size from 8" and 6" to a

manageable 4" and 3" for the two-phase inlet and water outlet, respectively. The air outlet from the separator is located at the very top to allow the air to escape from the separator. The air outlet has a 6" to 2" reducer and the outlet extends upwards another 18" above the separator to increase the water/air separation ability. A small flanged connection is used for a water outlet for the circulation pump.



Figure 4: Pipe reducer

Thermocouples are inserted in the lower and upper portions of the separator tank to record the temperatures of the water and air, respectively. A single pressure transducer

records the pressure of the separator tank. The level of water in the tank is monitored via a length of semi-clear plastic tubing that is affixed to the side of the separator and is connected to the separator on the top and bottom, as shown in Figure 5. While running experiments, periodic checks of the water tank level were performed to ensure seal flush flow was uninhibited. For safety, the separator was equipped with a 125 psi pressure relief valve.



Figure 5: Water level indicator tube

3.3 Twin-Screw Pump

The twin-screw pump used in this experimental rig to verify the results was a Colfax MR-200 twin-screw pump, shown in Figure 6.

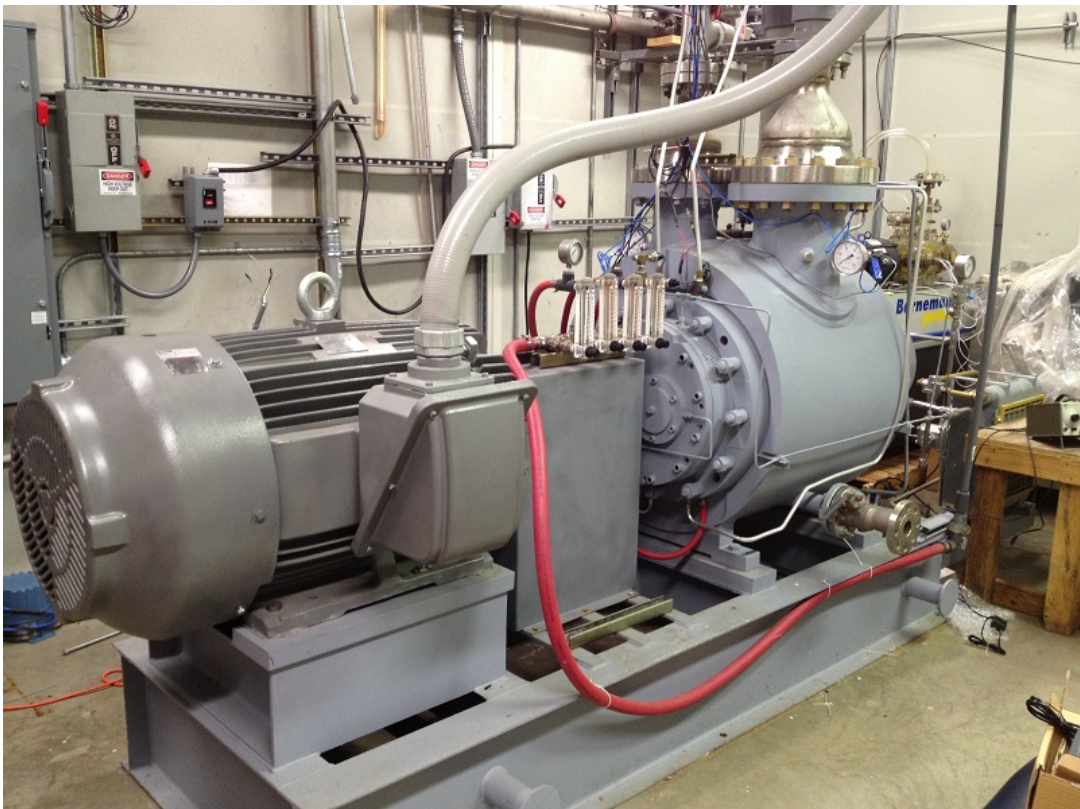


Figure 6: Colfax MR-200 twin-screw pump

The pump motor is a 200 hp 480V motor that provides the rotating power to turn the screws. The motor is connected to one screw and a set of timing gears transfers the angular motion to the second screw. The internal pump seals are lubricated at four points, each receiving 4 GPM of liquid for cooling and lubrication for a total of 16 GPM of seal flush. The seal flush flow is provided by the recirculation pump, and the flow

rate is controlled manually by four rotameters, shown in Figure 7. A secondary lubrication system is provided by an API Plan 52 reservoir. The unpressurized Plan 52 reservoir is located at a height above the pump, and utilizes the principles of natural convection to bring cool water to the lip seals and to evacuate warmer water away from the lip seals.

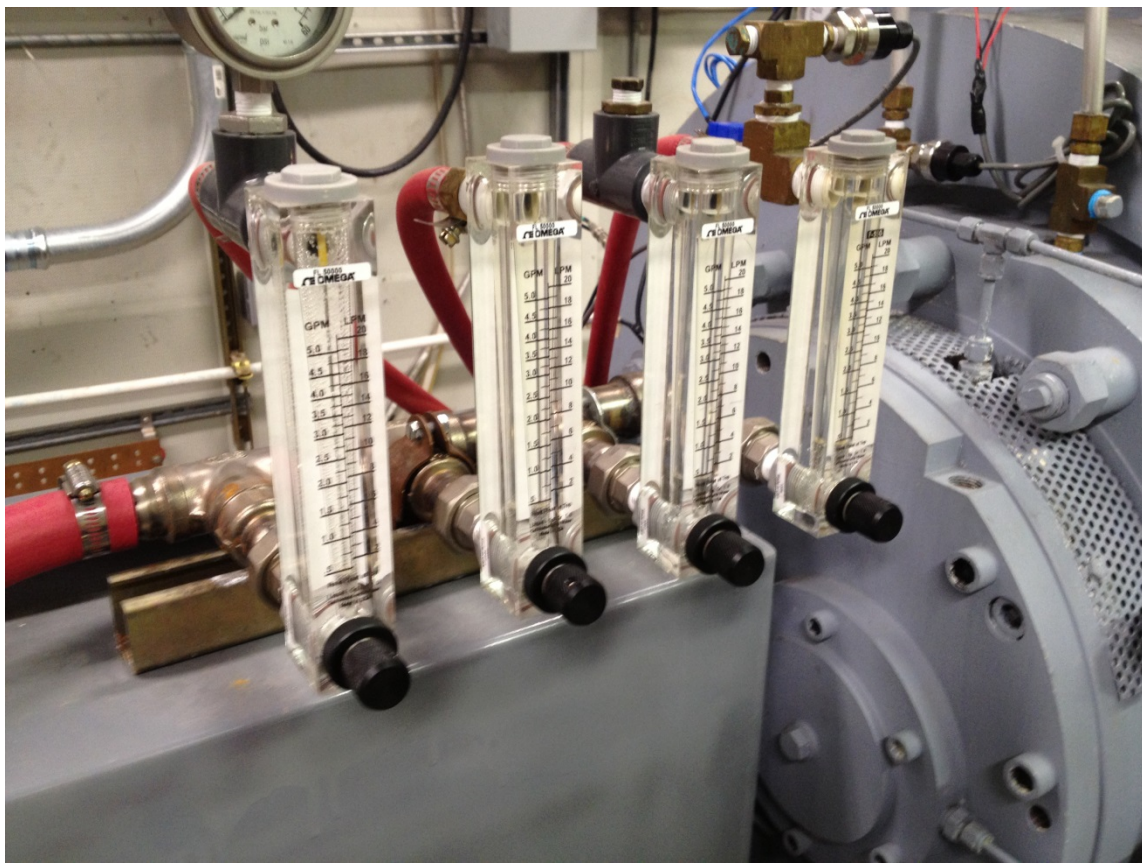


Figure 7: Rotameter flow control valves for seal flush

This 200 hp pump has a theoretical flow rate of 633 GPM, and can operate from 0.0 - 1.0 GVF, provided a minimum 16 GPM of liquid seal flush is maintained. The outlet of the

pump provides the separator with a two-phase mixture of water and air, which is then separated by gravity into distinct gas and liquid phases. For the purposes of verifying this test facility the pump was run at half speed, which equates to 900 RPM. This speed was chosen in part because the parameters of interest experience a greater range of variability at half speed than at full speed. Thus, testing at 900 RPM would provide more detailed indications of the equivalency of the old and new test facilities.

3.4 Circulation Pump

An external circulation pump is used to provide water for the seal flush as well as water for the heat exchangers. The circulation pump chosen is a ITT A-C 734+ Magnetic Drive Pump sized at 1.5x1x8, shown in Figure 8. The internal impeller diameter has a diameter of 6.75". The pump is powered by a 3,490 RPM 15 hp electric motor that utilizes a magnetic coupling to transfer the angular motion to the pump. The manufacturer's performance curves state that the pump can reach 80 GPM flow rate at a maximum differential pressure of 130 psi.

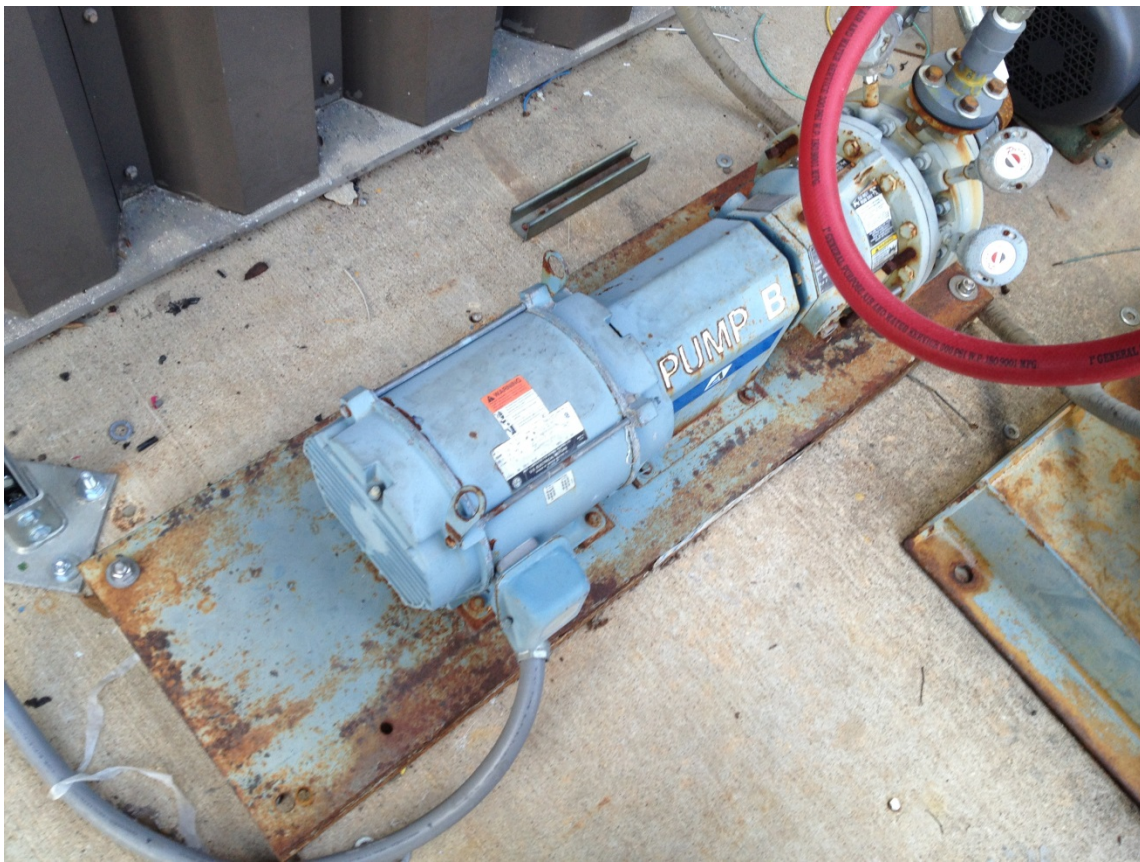


Figure 8: Circulation pump

The circulation pump is connected by a hose to a flanged connection near the bottom of the separator. A Y-strainer is positioned between the separator and the circulation pump to capture any large particles of corrosion. The circulation pump is then connected by a second hose to the two heat exchangers, as well as to the seal flush line.

3.5 Piping and Filtering

3.5.1 Piping

Due to financial constraints, a mixture of Schedule 40 carbon steel and Schedule 80 chlorinated polyvinyl chloride (CPVC) pipe was used for the main flow path, depending on cost and availability. Carbon steel pipe was used as much as possible due to its inherent higher resistance to temperature when compared with CPVC pipe. Already-existing Schedule 40 stainless steel pipe was used between the outlet of the pump and the outlet control valve to maintain the ability to perform tests at high outlet pressures.

Flexible water and air hoses were used for secondary flow paths to connect the heat exchangers and the seal flush lines. Flexible hoses with cam-lock fittings were used for the final section of flow path between the inlet control valves and the inlet of the pump. A mixture of Schedule 40 CPVC pipe and Schedule 40 stainless steel pipe was used for the air outlet line from the separator.

A total of five filtering devices were used in the flow path to protect the twin-screw pump, circulation pump, and heat exchangers from particles of corrosion. Due to extreme corrosion in the separator vessel, the water filter was rinsed out several times before running the twin-screw pump, thus avoiding major exposure of the pump to debris.

An air regulator was used for initial pressurization of the separator, shown in Figure 9.

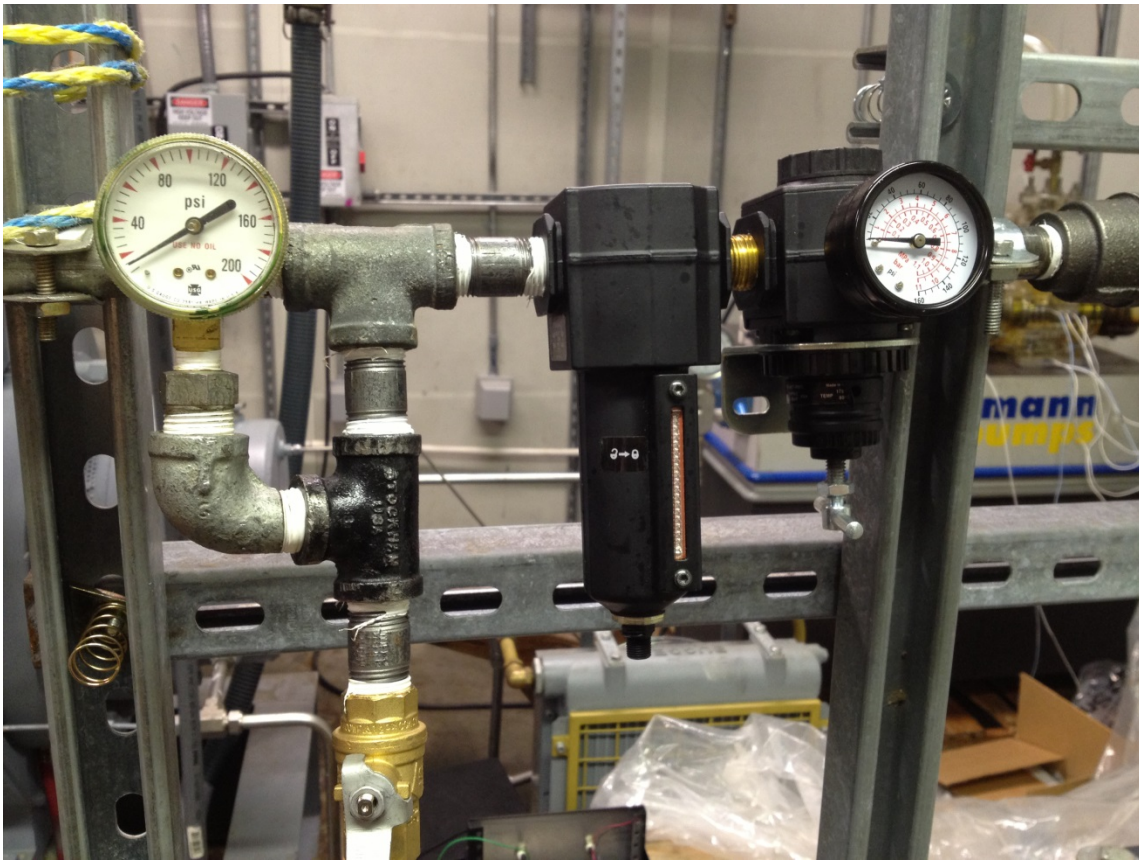


Figure 9: Air pressure regulator

3.5.2 Main Water Filter

A large Norman 8400 Series filter with a reusable 141 micron filter element was used on the main water outlet from the separator, shown in Figure 10. The twin-screw pump was run in short bursts several times to pull water through the filter. The filter was then cleaned before any experiments were run. The filter is limited to a pressure of 300 psi and a flow rate of 300 GPM when operating in a return line (100 GPM limit for a suction line). Since the separator is pressurized to a higher pressure than the pump inlet, this

causes the filter to operate as if it were in a return line. The temperature limit of the filter is 250°F.



Figure 10: Main water filter

3.5.3 Circulation Pump Y-Strainer

The circulation pump line (and thus the seal flush and heat exchangers) are protected by an 800 micron Y-strainer to prevent any larger particles of corrosion from proceeding further. The coarseness of the 800 micron Y-strainer allows smaller particles through, thus preserving the flow rate through the strainer and preventing a significant pressure

drop. The small particles that pass through the Y-strainer will not damage the heat exchanger tubing. The seal flush should not ingest these small particles, however, and is thus protected by a secondary filter.

3.5.4 Seal Flush Water Filter

The seal flush line is protected by a Pentek #10 Big Blue filter with a 50 micron reusable polyester filter element. The filter is located between the circulation pump and the seal flush rotameters. It also protects the Plan 52 non-pressurized reservoir when refilling. Without the filter, small particles of corrosion or other debris would be injected directly into the seals and the clearances of the pump, resulting in excessive wear on the internal parts.

3.5.5 Air Filters

Two 1" NPT air filters with automatic drain valves are used in parallel to provide a total maximum flow rate of 646 SCFM at 100 psi. The air filters capture particles down to 5 microns in size, and have clear bowls for the ability to visually check for debris or water ingestion. The automatic drain valves open when a float inside the filter detects a significant quantity of water.

3.6 Heat Exchangers

Two off-the shelf HVAC condensers were modified to perform as heat exchangers for the flow path, as shown in Figure 11. The compressor and electronic control circuitry was removed from each unit to leave the copper tubing, fins, and fan. New fan capacitors were obtained and the 220V motors were wired to an electric breaker to provide the fan power. The copper tubing connections were trimmed to length with a pipe cutter and copper pipe thread fittings were soldered on with an acetylene torch. The heat exchangers are connected in parallel to the water supply from the circulation pump, and discharge directly into the top of the separator near the two-phase inlet.

A rack was designed and built for the heat exchangers to lift them up off the ground and provide better air circulation. This aerial design also saved space for the new experimental facility as the heat exchangers are located 8' above existing equipment. This provided space to easily access the surrounding equipment for maintenance.



Figure 11: Heat exchangers and support structure

The rack itself was made of electrical support strut (also known as unistrut) and was fixed to the test facility building to provide extra stability. The base of the support structure was anchored to the slab with concrete anchor bolts. The heat exchanger structure was lifted into place with a fork lift, as shown in Figure 12.



Figure 12: Heat exchangers and support structure being lifted into place

3.7 Flow Control Valves

A total of five Masoneilan electro-pneumatic flow control valves were used in the flow system to control the inlet flow of water and air, as well as the exit flow. The valves operate by receiving 4-20mA signals from a National Instruments 9265 Analog Output Module card. The valves are powered by pneumatic pressure, which is supplied by the low-pressure shop air compressor. One valve is mated to each of the three water flow meters, as shown in Figure 13.



Figure 13: Water flow control valves

The air flow is controlled by a single 3" electro-pneumatic valve, as shown in Figure 14.

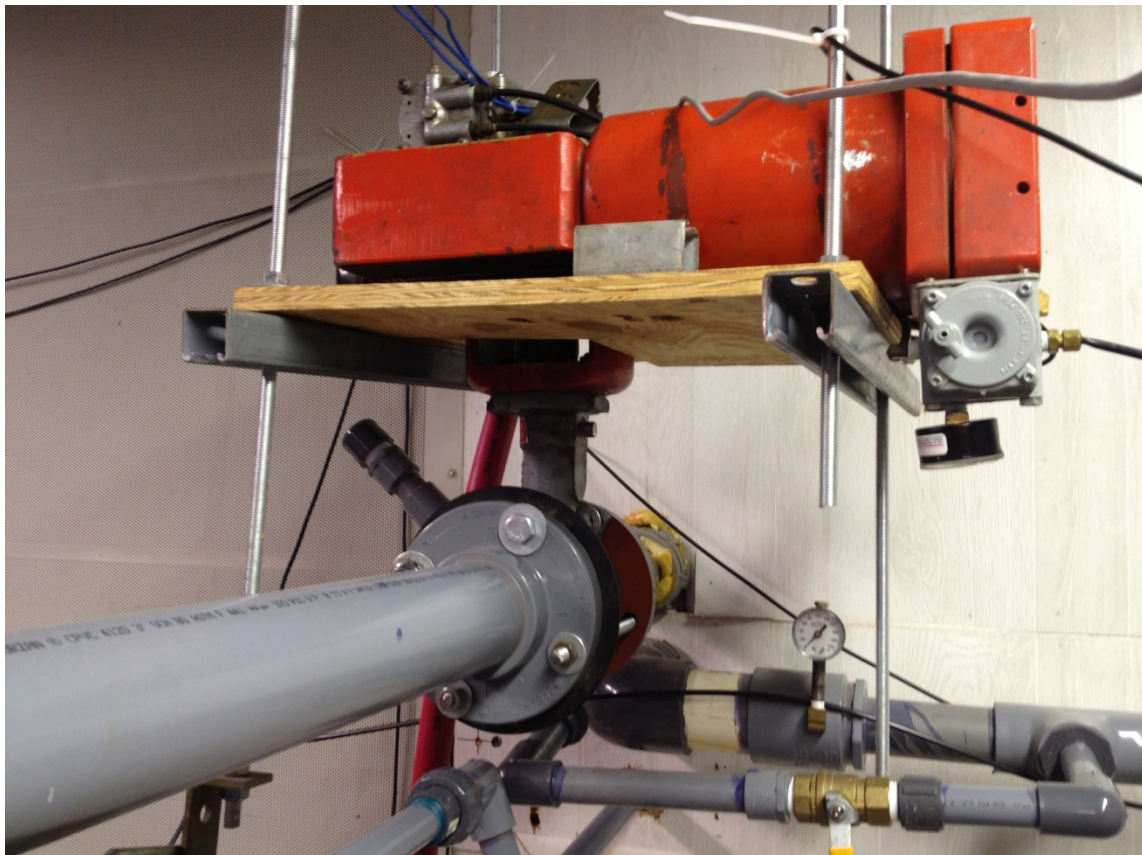


Figure 14: Air control valve

The outlet pressure of the pump is regulated by a single 3" control valve, as shown in Figure 15.



Figure 15: Outlet control valve

3.8 Flow Meters

Various turbine flow meters were used to calculate the flow rate at different points in the flow loop. These flow meters operate by means of a small turbine that is spun by the water or air as it passes through the flow meter. The turbine spins with an angular speed proportional to the volumetric flow rate of the fluid. This angular speed is converted to an alternating current frequency by means of a magnetic pick-up that senses when each turbine blade passes. This frequency is measured by an Omega iServer Microserver that provides the frequency output via an Ethernet cable to a computer for data analysis. The water flow meters are tabulated below in Table 2.

Table 2: Water flow meters

Equipment Model	Measurement Range	Uncertainty
Daniel Industries 1503-1D Flow Meter	22-225 GPM	$\pm 0.25\%$
Omega FTB-1425 Flow Meter	5-50 GPM	$\pm 1.00\%$
Omega FTB-1422 Flow Meter	0.75-7.5 GPM	$\pm 1.00\%$
Omega FTB-1425 Flow Meter (seal flush)	5-50 GPM	$\pm 1.00\%$
Omega iServer MicroServer	1Hz-100KHz	$\pm 0.30\%$

The air flow meter equipment used is listed in Table 3.

Table 3: Air flow meter

Equipment Model	Measurement Range	Uncertainty
Daniel Industries 2 Inch Gas Turbine Meter	10-100 CFM	$\pm 1.00\%$
Omega iServer MicroServer	1Hz-100KHz	$\pm 0.30\%$

A rotary flow indicator was used in the water line from the heat exchangers to ensure constant flow. The rotary flow indicator shown in Figure 16 was vital to give notice of blockages in the water line from the heat exchangers.



Figure 16: Rotary flow indicator

3.9 Instrumentation and Data Acquisition

3.9.1 Pressure Transducers

Seven Omega PX481A pressure transducers were used to monitor the pressure throughout the flow system, as shown in Figure 17. The pressure transducers operate by converting the pressure into an analog 1-5V DC signal. Pressure transducers used for gas volume calculations (where high accuracy was needed) were calibrated with a deadweight calibration system. A pressure transducer was used on the separator vessel to monitor pressure fluctuations inside the vessel and to ensure that the vessel pressure

was maintained comfortably below the limit of the pressure relief valve. A pair of pressure transducers was used before and after the air inlet control valve. This allowed the air flow meter to be placed upstream of the control valve, thus insulated from the inlet pressure fluctuations that occur as a result of the rotating pump. This allowed for a very stable measurement of the volumetric flow rate at the flow meter. The volumetric flow rate, used in combination with pressure and temperature sensor data, enables the calculation of the mass flow rate.



Figure 17: Pressure transducer at pump outlet

The pressure transducer scales, locations, and uncertainties are listed in Table 4:

Table 4: Pressure transducer locations

Location	Scale [psig]	Uncertainty
Pump inlet	0-200	$\pm 0.30\%$
Seal flush outlet		
Seal flush inlet		
Air flow meter		
Separator		
Air compressor supply		
Pump outlet	0-500	

3.9.2 Thermocouples

Seven thermocouples were used to measure the temperature of the air and water at various points in the flow path, an example of which is shown in Figure 18. Of particular importance were the temperature measurements at the pump inlet and exit (allowing the calculation of the increase of heat energy in the two-phase mixture), as well as the temperature measurement at the air flow meter allowing the calculation of the mass flow rate of air at the flow meter using the ideal gas law. The temperature in the separator is measured in two places. The gas temperature at the top of the separator is measured independently of the temperature of the water at the bottom of the separator. Monitoring the values of the temperature readings gave insight as to the effects of the heat exchangers, as well as to when the testing needed to be stopped to allow the CPVC pipes to cool.



Figure 18: Thermocouple

All thermocouples used to collect temperature data were Omega TQSS-116 T-type thermocouples, with specifications given in Table 5 .

Table 5: Thermocouple specifications

Equipment Model	Measurement Range	Uncertainty
Omega TQSS-116 T-type Thermocouple	32-662°F	±0.75%

3.9.3 Data Acquisition Modules

An NI 9213 Thermocouple Input Module with built-in cold-junction compensation was used to read the data from the thermocouples. A NI 9205 Analog Input Module was used to receive the voltage signals from the pressure transducers. A NI 9265 Analog Output Module was used to provide a 4-20 mA signal to the flow control valves. Three iServer Microservers shown in Figure 19 were used to analyze the frequency output data from the turbine flow meters and transmit the results via an ethernet connection to the computer.



Figure 19: Omega iServer microservers

The specifications for these modules are found in Table 6.

Table 6: Data acquisition modules

Equipment Model	Measurement Range	Uncertainty
NI 9213 Thermocouple Input Module	± 78.125 mV	$\pm 0.30\%$
NI 9205 Analog Input Module	± 10 V	$\pm 1.00\%$
NI 9265 Analog Output Module	0-20 mA	$\pm 2.50\%$
Omega iServer Microserver	1Hz-100KHz	$\pm 0.30\%$

3.9.4 LabVIEW Program

All data acquisition was achieved through the National Instruments LabVIEW computer program. A program was written to incorporate recording temperature, pressure, and flow meter data, as well as to perform calculations on the data. A PID controller was created within LabVIEW to manipulate the control valves, shown in Figure 20. The inlet pressure, outlet pressure, and GVF could be specified by the user, and the program would respond accordingly by gradually opening or closing valves until the desired settings were achieved.

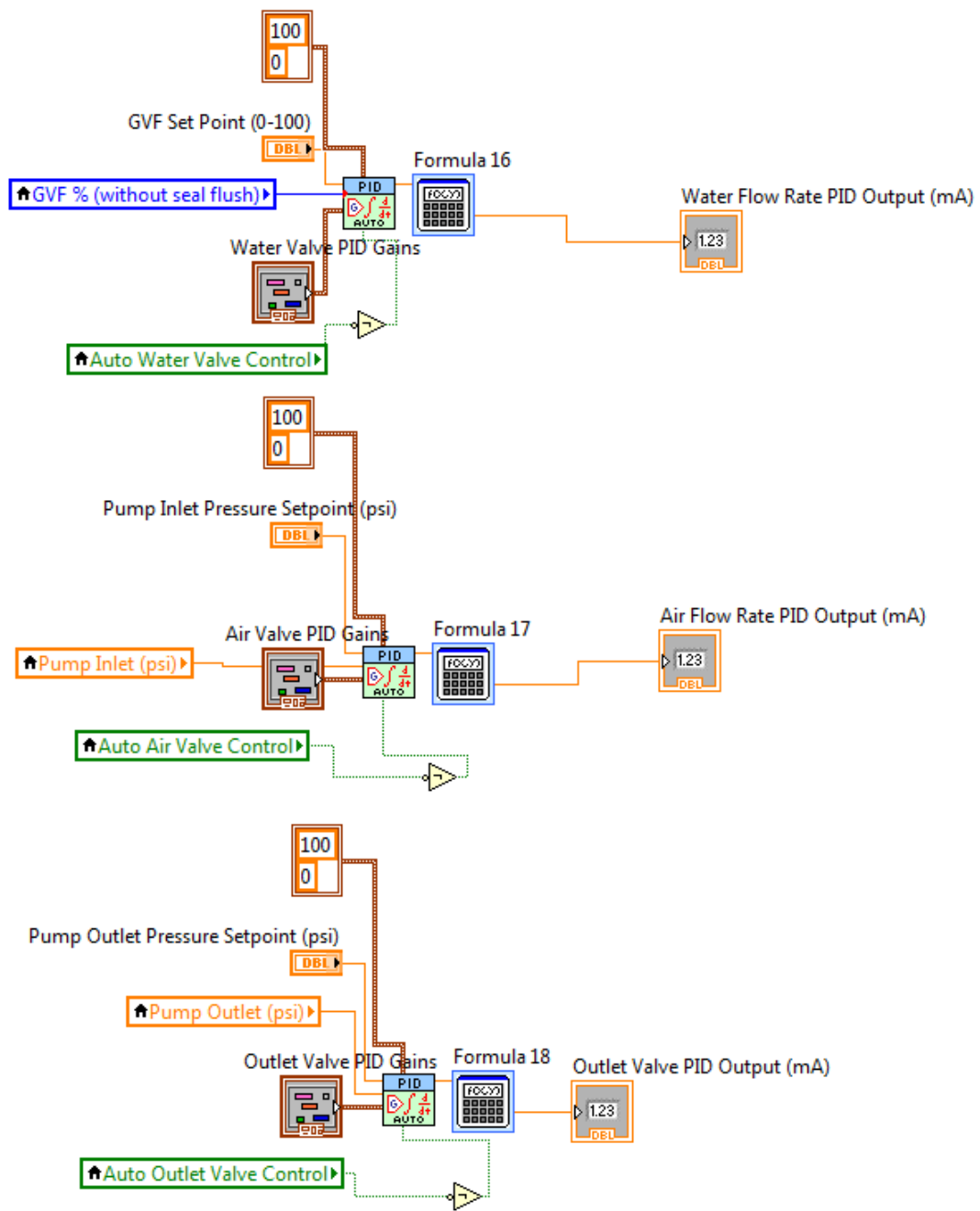


Figure 20: LabVIEW PID control

The program was written in such a way that the user can manually control the valves, as shown in Figure 21. This manual control was particularly useful when first starting the pump as all the valves could be set fully open/closed depending on the requirements.

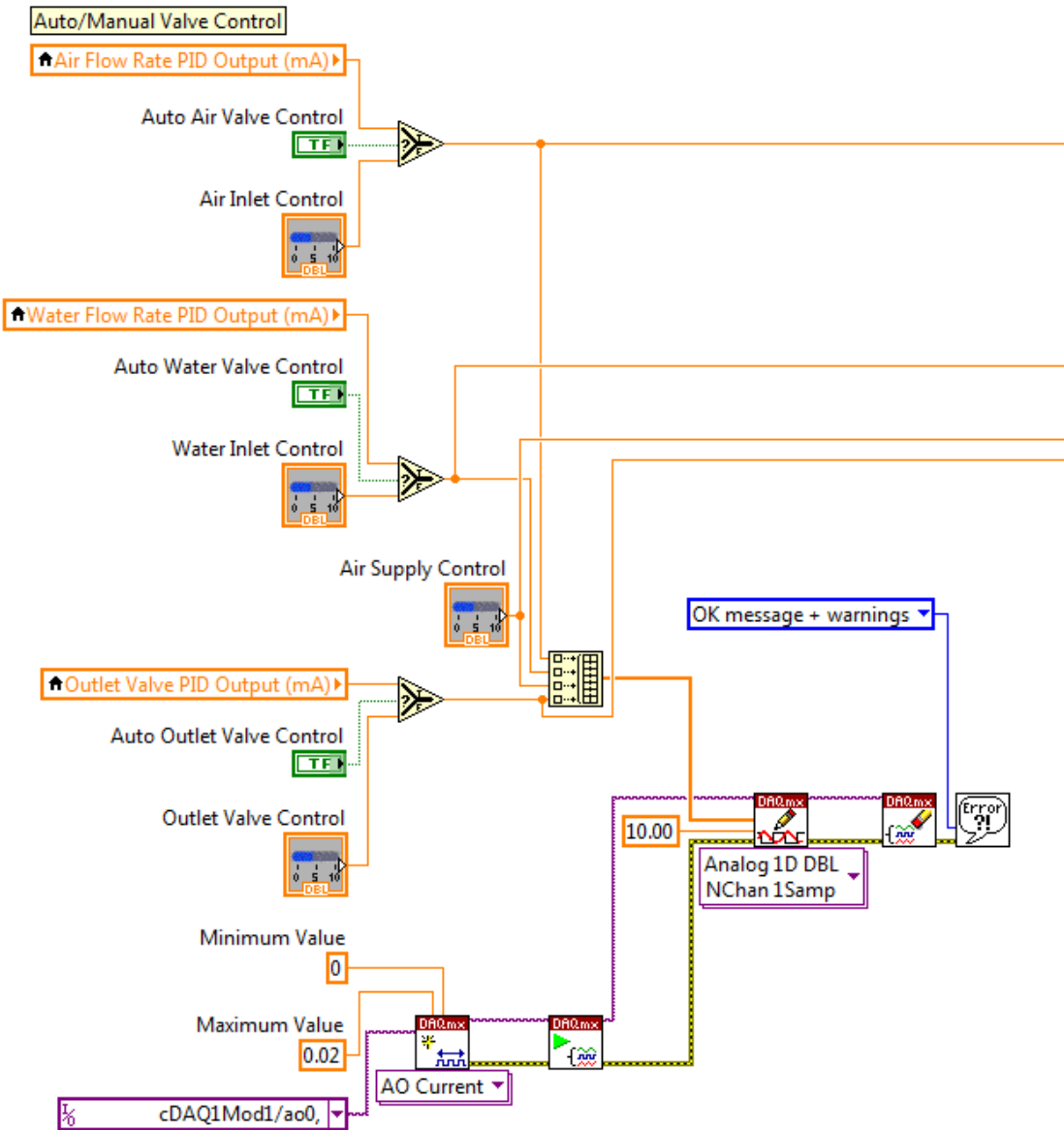


Figure 21: LabVIEW valve control

The program was written to read all the temperature and pressure data while simultaneously using the ideal gas law to calculate the volumetric flow rates at the pump inlet, and then the GVF, shown in Figure 22.

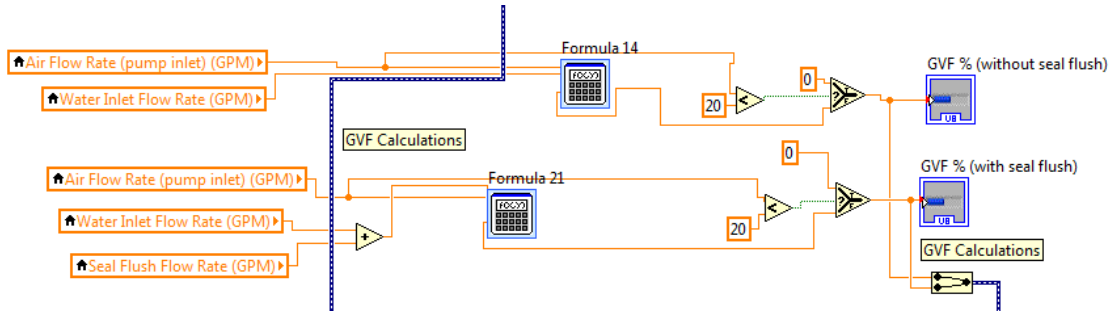


Figure 22: LabVIEW GVF calculations

Warning lights were incorporated into the LabVIEW program to warn the user when certain sensors dropped below specified values, shown in Figure 23. The most critical of these was the seal flush flow meter, which was required to have a flow rate of at least 16 GPM. Warning lights were also added for the separator for pressure and temperature monitoring. A warning light for the volumetric flow rate at the flow meter was also added to ensure that the flow rate did not exceed the maximum flow rate of the flow meter to prevent over spin and subsequent damage to the flow meter.

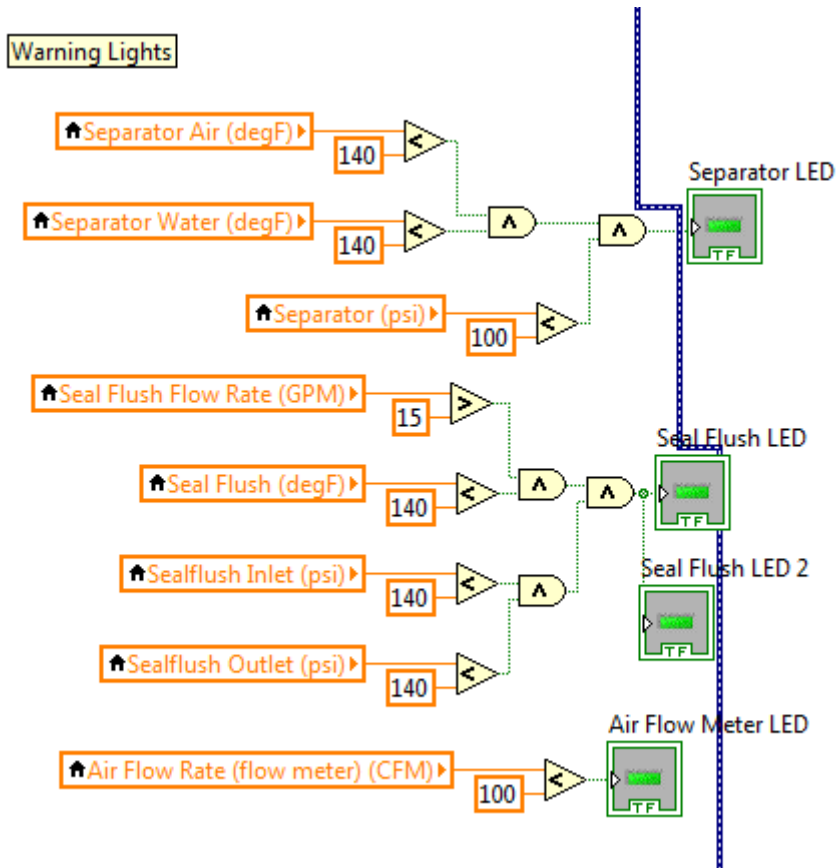


Figure 23: LabVIEW warning lights

The front panel of the LabVIEW program was designed to aid the user in quickly accessing the required information and making adjustments easily. The front panel of the program spanned two computer monitors to give the greatest surface area for monitoring and control. Screenshots of the front panel can be found in Figure 24 and Figure 25.

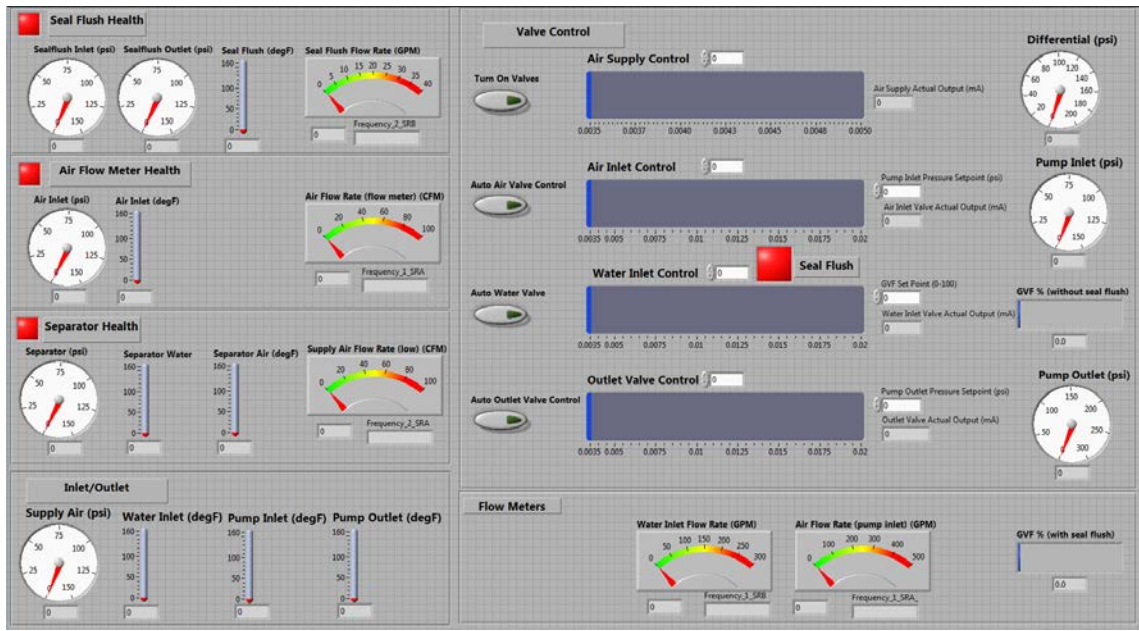


Figure 24: Left side of front panel of LabVIEW program

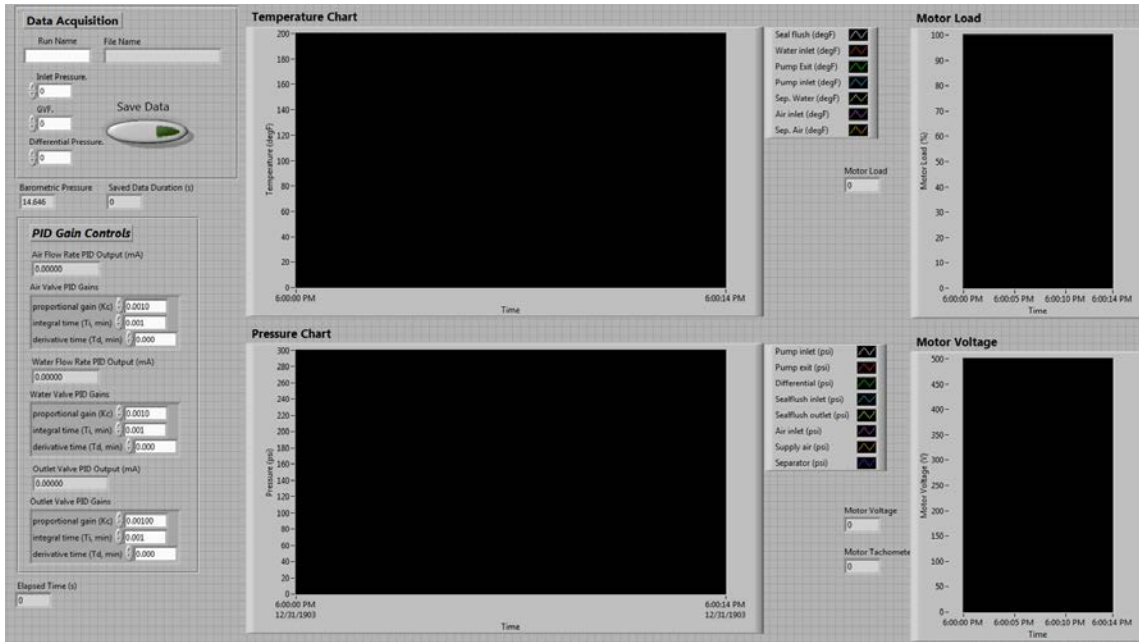


Figure 25: Right side of front panel of LabVIEW program

3.10 Electrical Power System

The mechanical twin-screw pump was driven by a 200 hp Westinghouse 460V electric motor. The motor's electrical power was supplied by a Dynamatic AF5000+ Variable Frequency Drive (VFD), shown in Figure 26.



Figure 26: Variable frequency drive

The electrical power for the heat exchanger fans was supplied directly from a 220V electrical breaker.

The electrical power for the 15 HP circulation pump was supplied from a 460V breaker in series with a pump starter.

3.11 Method of Operation

The following set of instructions was created to aid in the proper operation of the experiment, as well as to provide direction for future users of the test facility.

3.11.1 Start Up Procedure

1. Check oil level in the gearbox
2. Check water level in Plan 52 reservoir (level with mark on sight glass), fill as necessary (use circulation pump to pressurize seal flush line)
3. Check water level in separator (50%-75% full), fill as necessary
4. Start oil free air compressor (follow instructions in manual) for air supply
5. Start shop air valve in test cell to power electro-pneumatic valves
6. Close two inch air line ball valve (to protect air turbine meter from water leakage during startup)
7. Start Labview program (Outlet valve open, inlet valves closed)
8. Pressurize separator tank to desired pressure (max of 100 psi for safety)
9. Check functionality of all sensors and valves in Labview

10. Start heat exchanger fans
11. Start circulation pump
12. Set seal flush inlet flow to 16 gpm total (4 gpm each Rotameter)
13. Turn the VFD power on and set to desired speed (15Hz for startup)
14. Open water inlet valve and pump outlet valve all the way, while simultaneously pressing the green “Start” button on the VFD outside the test cell (have a second person do this)
15. Open two inch air line ball valve
16. Switch valve controls to automatic, gradually opening air valve to set the inlet pressure
17. Gradually increase frequency of the VFD drive

3.11.2 Pump Operation Procedure

1. Ensure that the seal flush flow rate stays above 16 gpm
2. Ensure that the separator pressure stays below 100 psi (hose and pipe limitation)
3. Avoid contact with gearbox or other rotating parts
4. Ensure all other pressures are within safe levels

3.11.3 Pump Shut Off Procedure

1. Open outlet valve completely
2. Press “Stop” button on control box while closing the inlet valves to the pump
3. Stop VFD

4. Stop circulation pump
5. Stop heat exchanger fans
6. Stop air compressor
7. Stop shop air supply

4 CONSTRUCTION AND ASSEMBLY

4.1 Separator

The separator was moved from storage to the new test facility via a forklift. Once in the new location, the separator was anchored to the concrete slab using $\frac{3}{4}$ "x 6" concrete anchor bolts. The surface corrosion on the separator flange faces was ground off with a hand grinder, while attempting to preserve the circular gasket grooves. The separator was pressurized and depressurized several times and rinsed with water to dislodge as many rust particles as possible. The circulation pump was run continuously for several hours to recirculate water and dislodge more particles.

4.2 Piping and Control Valves

Existing piping and control valves were used whenever possible, as the main parts being modified were water and air supply sources, not the supply lines themselves.

To reduce the large flange connection size of the separator to the desired system pipe size of 3"-4", flanges and reducers were cut out of existing stock with an acetylene torch. The flanges and reducers were then machine welded at a local welding shop to produce the reducing pipe spools. An existing reducer was used to reduce the air outlet of the separator to a 2" pipe size.

The separator water outlet was piped to an existing water line using a short length of 3"

CPVC pipe. The existing line was cut, and a 3" tee was put in place to receive the water line from the separator.

The previous system had no air line from the separator area (as the air was previously drawn from the compressors, with covered permanent piping to the test cell). However, there were two existing water lines for low volumetric flow water and high volumetric flow water, respectively. The low flow line was chosen to be used for water, as it was already piped to three turbine flow meters that operated over a large range. This left the high flow line unused. The high water flow rate electro-pneumatic valve was to be used for the air line. In the interest of leaving the valve in its place, the air outlet from the separator was piped to the high water flow line, and manual valves were put in on the water supply and air supply to switch the flow from water to air and back again. For the purposes of this testing, only air was used in this line.

The two-phase outlet of the pump previously used 4" CPVC pipe to connect the pump outlet to an unpressurized water tank. The old pipe was removed and a new section of CPVC pipe was made to take its place and redirect the flow to the pressurized separator.

4.3 Heat Exchangers and Circulation Pump

The two heat exchangers were created from repurposed off-the-shelf HVAC condensers. The compressors were removed from each unit to leave only the fan and copper tubing, as shown in Figure 27.



Figure 27: Compressor removal from HVAC unit

Hose fittings were silver-soldered on to the inlet and outlet copper tubing connections on each heat exchanger. The soldered connections for the heat exchangers were initially

pressure tested with water to 70 psi, and all leaks were fixed. The copper tubing is rated to withstand pressures up to 300 psi.

The heat exchanger support structure was built to elevate the heat exchangers to 8 feet above the ground. This elevation gave the heat exchangers more air circulation, as well as extra space below the heat exchangers for other equipment. The support structure was made out of 1 5/8" square unistrut (commonly used in hanging cable channels/ductwork). The support structure and elevation can be seen in Figure 28.



Figure 28: Installation of heat exchanger support structure

Once lifted into place, the water and electrical connections were made. The inlet and outlet water connections were made with 1" general purpose reinforced air and water hose that can withstand pressures up to 300 psi. The two phase 220V electrical connections were made directly to a circuit breaker for ease of turning the fans on and off, as shown in Figure 29.



Figure 29: Circuit breaker for heat exchanger fans

The circulation pump provides the motive power to move the water through the heat exchangers, as well as move water through the twin-screw pump seal flush. The electrical power for the circulation pump comes from a 460V circuit breaker and motor starter, shown in Figure 30.



Figure 30: Circuit breaker and motor starter for circulation pump

5 RESULTS

5.1 Closed-loop Results

The closed-loop test was run at 15 psi and 50 psi inlet pressure, with GVF ranging from 0.65-0.92 and differential pressures ranging from 50-300 psi. Each data point was derived from 15 seconds of data that was averaged to produce a single data point. After each valve adjustment the system was given at least 30 seconds to reach equilibrium, and steady conditions were verified with a continuously updating graph of the system pressures and temperatures.

During testing at the higher differential pressure ranges, the air pressure in the separator would drop by up to 10 psi. This is due to the extra mass of air that was compressed in the outlet pipe between the pump outlet and the outlet valve. To experiment with the behavior of the system under high pressure conditions, the air supply for the test was handled in two ways. During the first part of the test, the air supply line from the compressors to the separator was opened and a pressure regulator was used to add air into the system when necessary to keep the separator pressure constant . During the second part of the test, the air supply line from the compressors to the separator was closed, thus turning the system into a true closed-loop system. A 25 psi oscillation was observed in the pump outlet pressure, as well as a smaller 5 psi oscillation in the pump inlet pressure. The oscillation was very steady and predictable, with the appearance of a sine wave with a period of about 3 seconds in most cases. It was also observed that

maintaining a steady system pressure with the open air supply line and pressure regulator decreased the magnitude of the outlet pressure oscillations, and almost completely damped the inlet pressure oscillations. The PID control for the outlet valve was ruled out as a factor. The controller was adjusted to respond to the outlet pressure at different rates, and pulsations continued. The outlet valve was even set to a constant value, and the pulsations continued to occur. It is recommended that a type of pulsation damper/accumulator on the pump outlet be used for future testing in this facility. A more detailed discussion and further recommendations are found in Section 6.2.

Periodic visual observations of the clear air filter bowls in the air line between the separator and the pump inlet were conducted to detect any signs of liquid carryover into the air line. No liquid was observed in the air filters during testing. After conducting the pump testing, the air filter bowls were removed and visually inspected. The bowls showed absolutely no signs of detectable moisture.

Upon first analysis of the data, discrepancies were observed between the results from the new test facility and the previous test facility. It was quickly determined that calculating the GVF solely by examining the process fluid without taking into account the recirculating seal flush affected the results considerably if the seal flush flow rate was different by even a 1-2 GPM. Therefore, the GVF shown in the following figures was calculated including the seal flush flow rate in the water flow rate equation.

5.1.1 Volumetric Efficiency

The volumetric efficiency of the pump is given as the ratio of the ideal volumetric flow rate (a function of the pump geometry) to the actual volumetric flow rate as shown in the equation below.

$$\eta_V = \frac{Q_a}{Q_{th}} \quad (7)$$

The pump contains clearances between the drive screws and the casing, and as flow leaks back through the clearances, the volumetric efficiency is decreased. These clearances are of a fixed geometry, and the cross-sectional area of the clearances can affect the volumetric efficiency of the pump if the leakage flow becomes choked. The pump was run at a half of full speed, therefore the theoretical volumetric flow rate was also halved. Because the cross-sectional clearance area is constant, the reduction in speed increased the range of volumetric efficiencies under which the pump clearances do not experience choked flow. The volumetric efficiency of the pump at 15 psi inlet pressure is given in Figure 31.

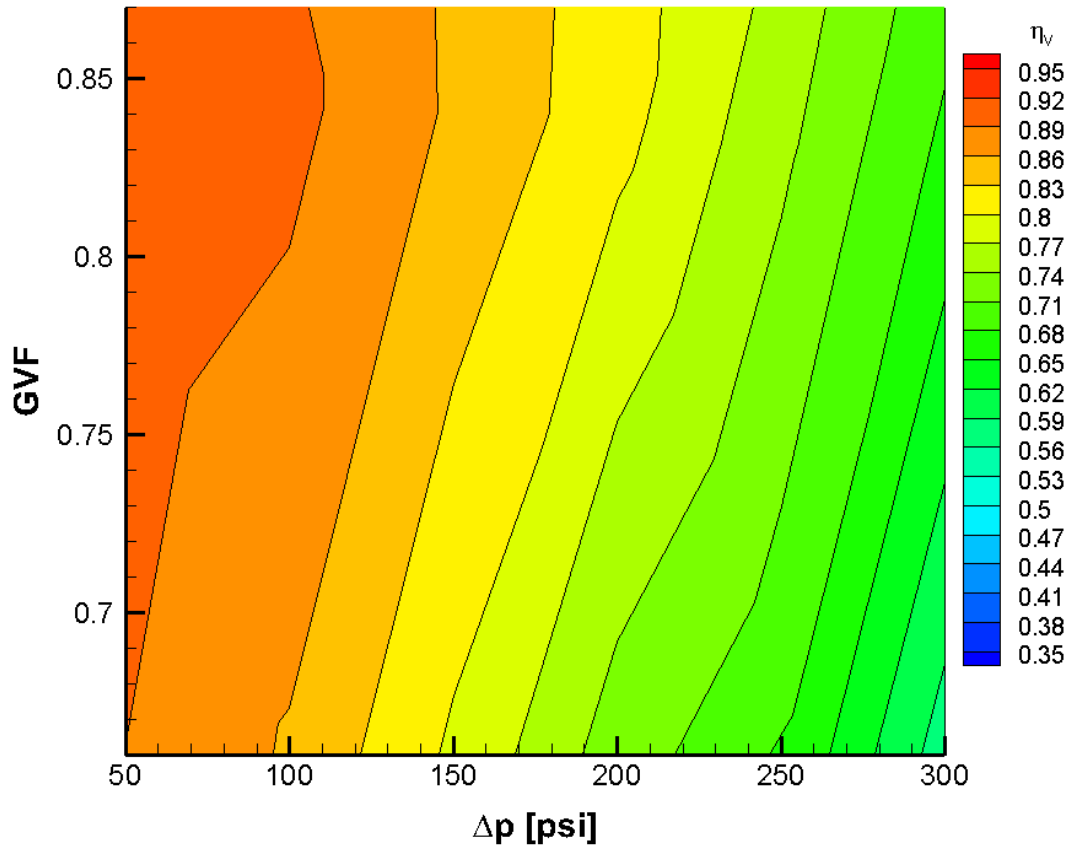


Figure 31: Volumetric efficiency at 15 psi inlet pressure and 900 RPM

As shown in Figure 31, the highest volumetric efficiency for this inlet pressure occurs at a high GVF and low differential pressure. As the Δp across the pump is increased, the higher pressure air becomes more difficult to compress, and the increased pressure induces a larger leakage flow through the clearances. As the leakage flow rate increases, the volumetric efficiency decreases.

The volumetric efficiency of the pump at 50 psi inlet pressure is shown in Figure 32.

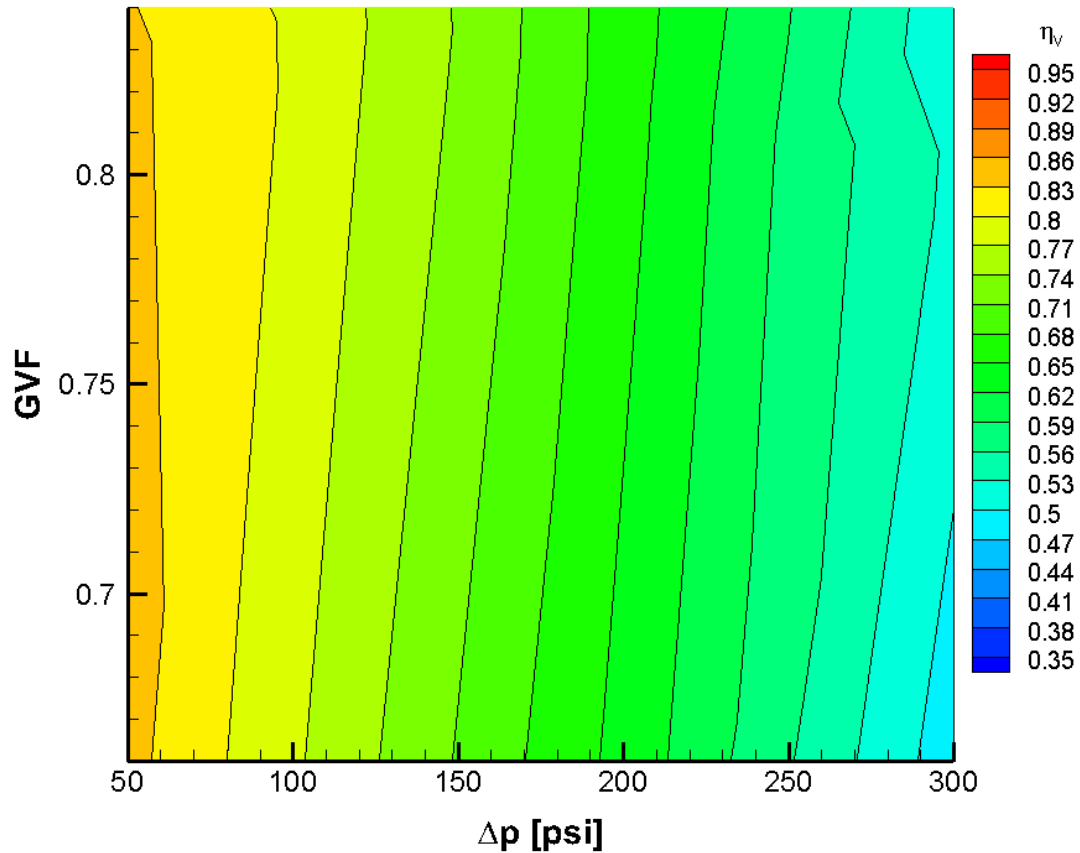


Figure 32: Volumetric efficiency at 50 psi inlet pressure and 900 RPM

As shown in Figure 32, the volumetric efficiency is less dependent on the GVF of the process fluid, and is more dependent on the differential pressure of the pump. This is caused by the higher inlet pressure, where the semi-compressed air induces a larger backflow through the clearances of the pump, and thus increases the leakage flow rate. Comparing Figure 31 and Figure 32, it can be seen that the pump inlet pressure plays a significant role in the volumetric efficiency of the pump, particularly at high gas volume fractions.

5.1.2 Mechanical Efficiency

The mechanical efficiency of the pump is the ratio of the power imparted to the fluid to the total electric power supplied to the pump, as shown in the below equation.

$$\eta_M = \frac{P_p}{P_e} \quad (8)$$

It should be noted that the pump power was modeled as isothermal, due to a maximum temperature rise of 10°F through the pump. The temperature rise in most cases was 2 - 3°F. The low temperature rise at high GVF is primarily due to the fact that the pump was operated at half speed. The mechanical efficiency at 15 psi is shown in Figure 33.

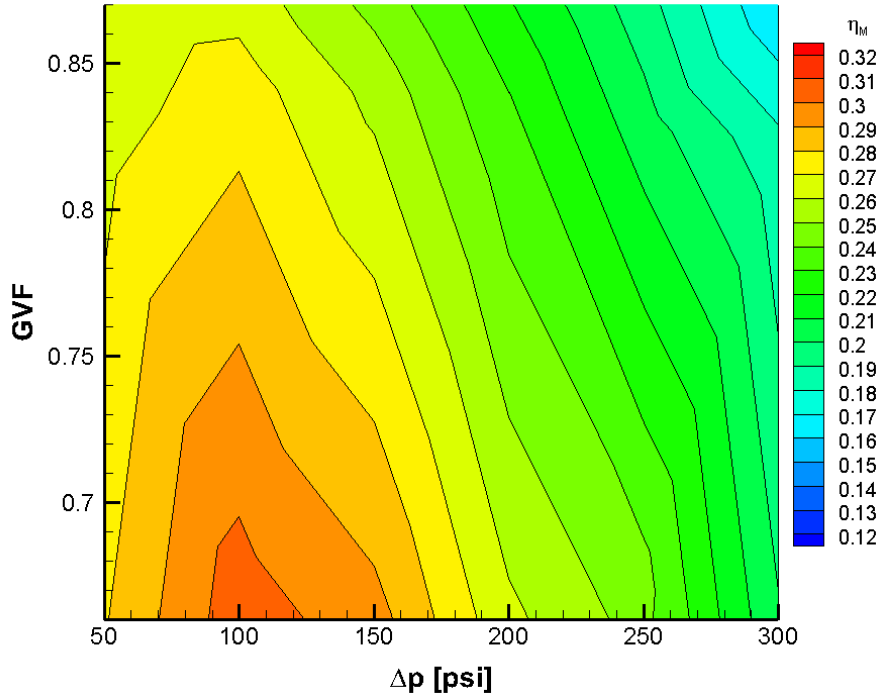


Figure 33: Mechanical efficiency at 15 psi inlet pressure and 900 RPM

The mechanical efficiency of the pump increases as the GVF decreases, as the pump is able to transmit a larger amount of energy to the water than to the air. The mechanical efficiency performance peaks at a differential pressure of 100 psi. The mechanical efficiency is strongly related to the differential pressure across the pump, and as such, care should be taken to choose the correct pump for the correct application.

The mechanical efficiency of the pump at 50 psi inlet pressure is shown in Figure 34.

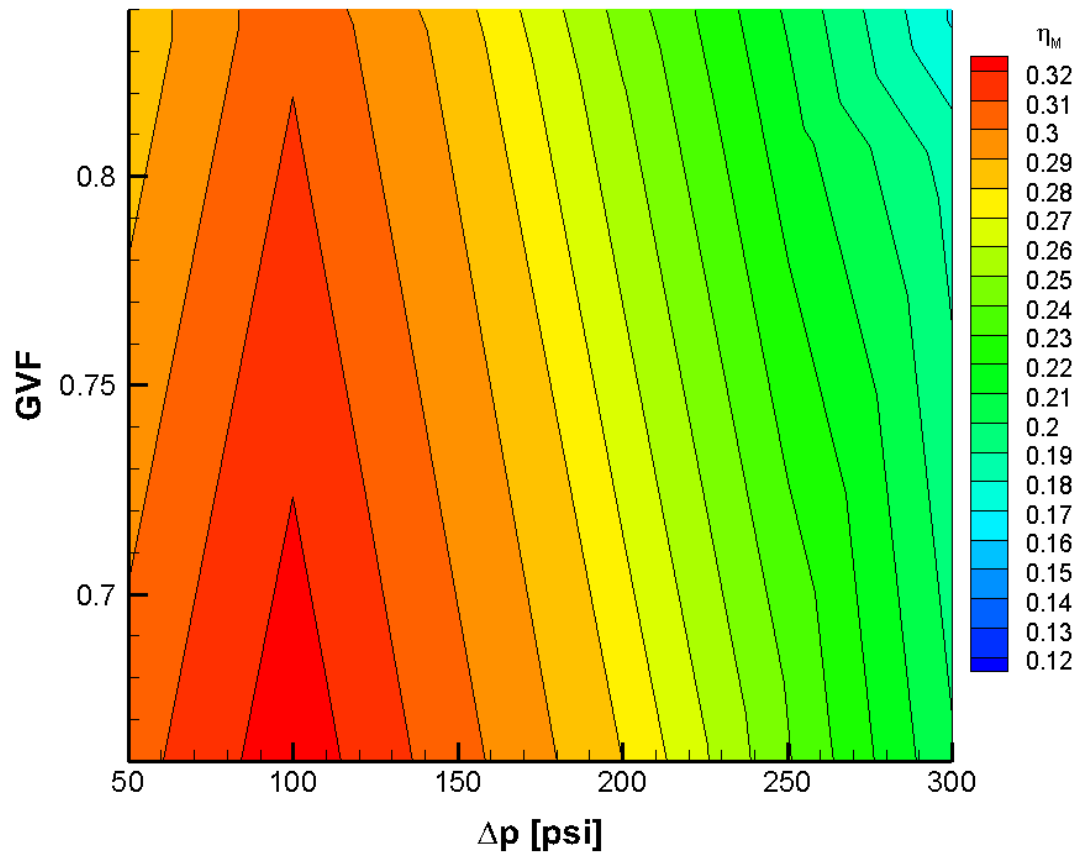


Figure 34: Mechanical efficiency at 50 psi inlet pressure and 900 RPM

As shown in Figure 34 the mechanical efficiency remains inversely related to GVF, with the efficiency increasing as GVF lowers. However, a much stronger peak is seen in the case of 50 psi inlet pressure compared to the 15 psi inlet pressure. At 50 psi inlet pressure, the working fluid becomes less compressible when compared to the 15 psi inlet pressure in Figure 33. An analysis of this reduction in compressibility is given by the pump effectiveness in Section 5.1.3, which characterizes the difference between the actual fluid and an ideal, incompressible fluid. As the Δp increases, the gas is compressed more and a higher leakage flow rate occurs, contributing to the lower mechanical efficiency at high Δp in Figure 33 and Figure 34.

This suggests that as the inlet pressure of the pump increases, it becomes more and more vital to run the pump at a particular differential pressure if maximizing the mechanical efficiency (and thus lowering electrical costs) is of interest.

5.1.3 Effectiveness

The effectiveness of the pump is defined as the ratio of the net power imparted to the compressible multiphase fluid and the power added to an incompressible fluid of identical volume.

$$\eta_{eff} = \frac{P_p}{P_h} \quad (9)$$

As the gas volume fraction increases, the pump experiences a reduction in the ability to impart energy into the working fluid, due to the reduced compressibility of the gas. The

effectiveness parameter characterizes this reduction in the ability to transfer energy to a fluid. It is solely a thermodynamic parameter, and is independent of pump type and geometry. This is in contrast to the mechanical and volumetric efficiency parameters, which are in fact affected by pump design and geometry. The pump effectiveness at 15 psi inlet pressure is shown in Figure 35.

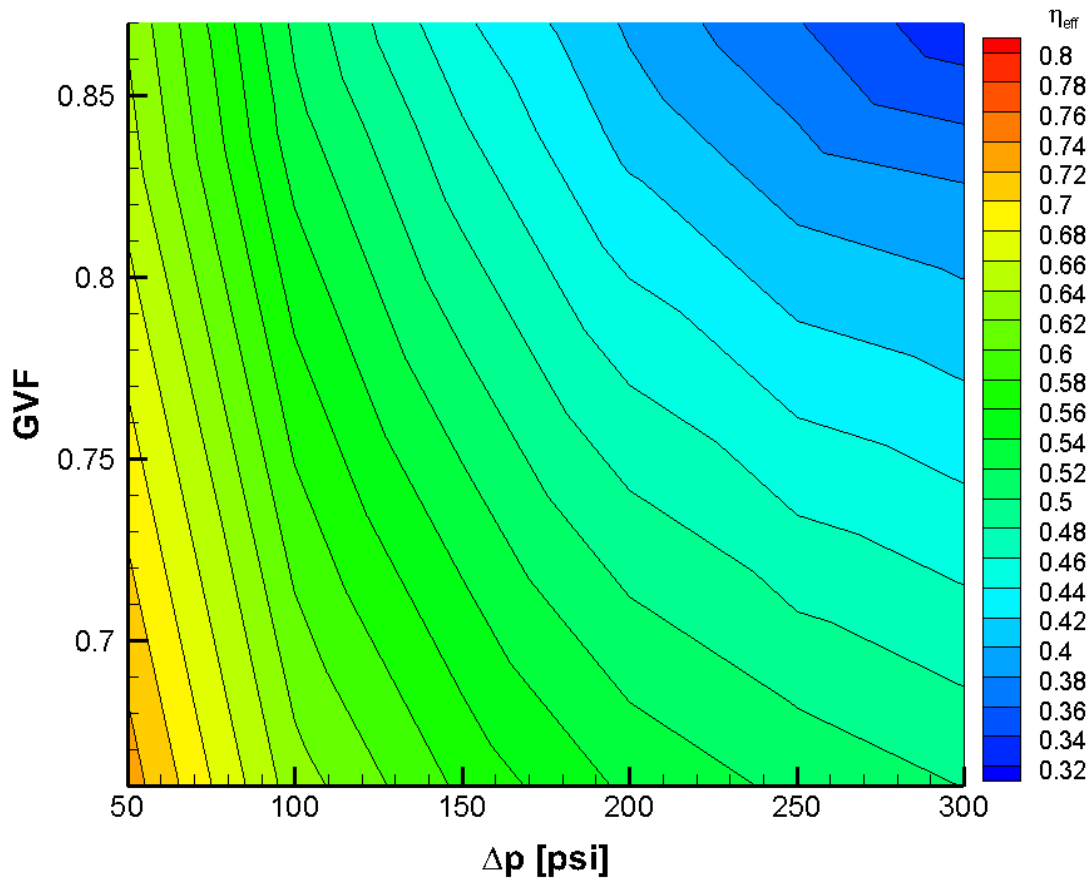


Figure 35: Pump effectiveness at 15 psi inlet pressure and 900 RPM

The effectiveness of the pump clearly increases as the differential pressure and GVF decrease. To understand this phenomenon, the fluid power equations for gas and liquid must be analyzed.

The power stored by a gas during compression is given in the isothermal case by:

$$P_{\text{gas}} = p_{\text{in}} Q \ln \left(\frac{p_{\text{out}}}{p_{\text{in}}} \right) \quad (10)$$

Therefore with increasing pressure the gas power grows logarithmically as shown in Figure 36.

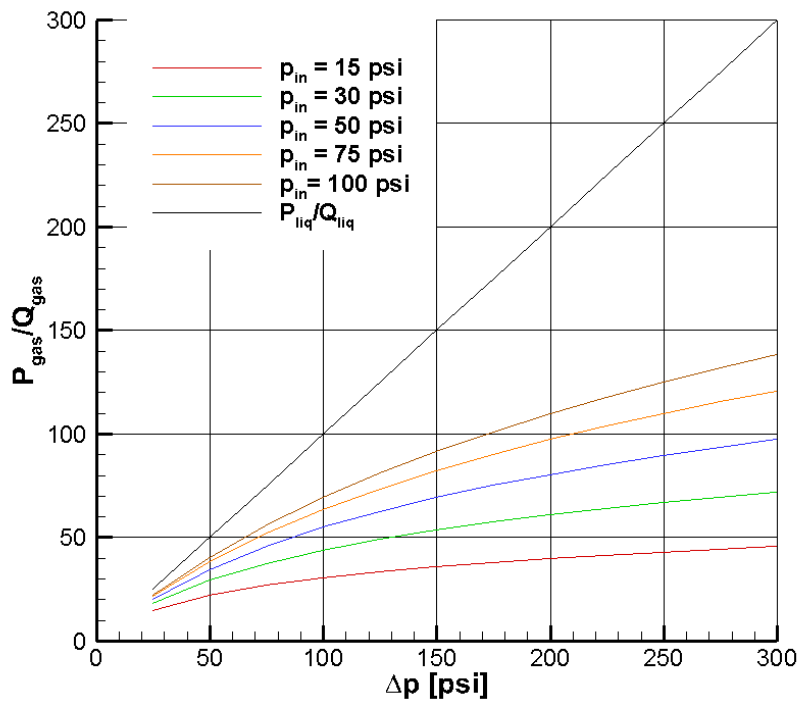


Figure 36: Logarithmic increase in power in isothermal gas compression

The power stored by a liquid during compression can be characterized by:

$$P_{liq} = Q\Delta p \quad (11)$$

Therefore the power stored by the liquid during compression increases linearly with respect to differential pressure, while the power stored by a gas increases logarithmically with differential pressure. The ratio of the liquid power to gas power is given by:

$$\frac{P_{liq}}{P_{gas}} = \frac{\Delta p}{p_{in} \ln\left(\frac{p_{out}}{p_{in}}\right)} > 1 \quad (12)$$

Therefore, it can be seen from the above equations that the power stored in a liquid at a fixed volumetric flow rate is the maximum power possible for a given flow rate and differential pressure. Any insertion of gas into the fluid (at the same flow rate and differential pressure) will decrease the amount of power that can be imparted to the working fluid.

To summarize, at higher GVF the effectiveness of the pump is decreased due to the inherent inability of the greater gas fraction to store the same power as the same volume of liquid.

The pump effectiveness at 50 psi is shown in Figure 37.

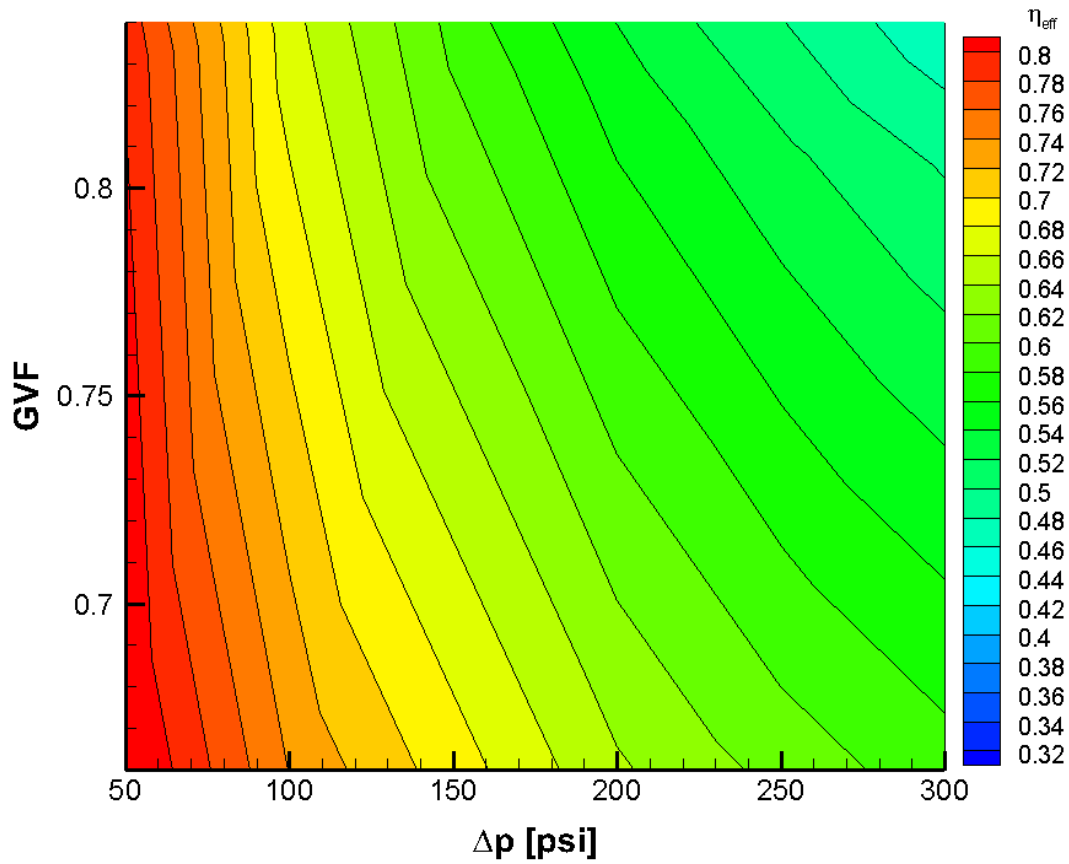


Figure 37: Pump effectiveness at 50 psi inlet pressure and 900 RPM

Clearly, the pump effectiveness has increased as the inlet pressure increased from 15 psi to 50 psi. This is due to the fact that gas enters the pump at a higher pressure, and thus at a reduced compressibility. As the inlet pressure of the pump increases, the pump experiences a compression process that is nearer to the ideal incompressible liquid process. Therefore, as the inlet pressure increases or as GVF decreases, the pump effectiveness increases.

5.2 Comparison with Previous Facility

Three parameters are used to compare the results of the new closed-loop test facility with the previous open-loop test facility. The calculated volumetric efficiency, mechanical efficiency, and effectiveness of the pump are compared as tested in each facility. Data was compared at 15 psi and 50 psi inlet pressures.

As mentioned in Section 5.1, the GVF calculation used to create the graphs includes the seal flush in the water flow equation, lowering the effective GVF while maintaining an accurate comparison between the previous facility and the new facility.

5.2.1 Volumetric Efficiency

The volumetric efficiency of the pump at 15 psi is shown in Figure 38 and Figure 39. As can be seen in Figure 38, the volumetric efficiency of the pump was slightly greater in the new facility than in the old facility. Part of the variation is likely due to the uncertainty in the volumetric efficiency measurement. The maximum uncertainty in the volumetric efficiency measurement at 15 psi inlet pressure found to be 1.25%. A detailed analysis of the uncertainty can be found in Appendix A.

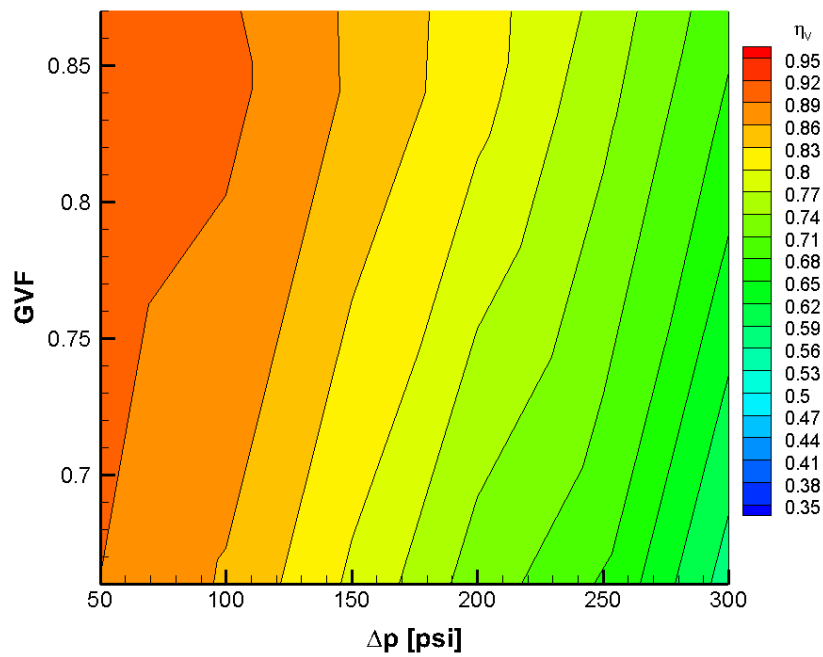


Figure 38: Volumetric efficiency in new facility (15 psi inlet, 900 RPM, 100°F)

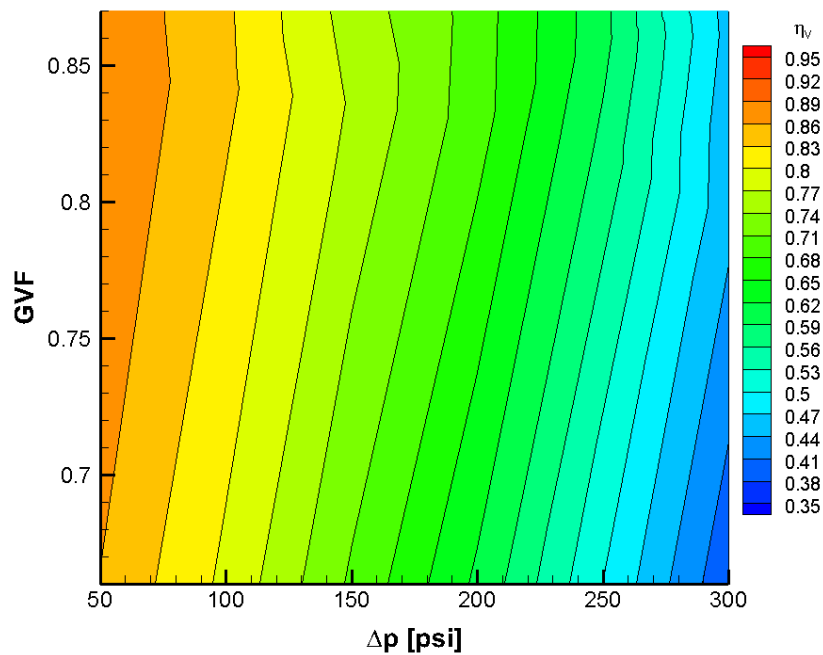


Figure 39: Volumetric efficiency in previous facility (15 psi inlet, 900 RPM, 75°F)

Another parameter affecting volumetric efficiency is the lack of temperature control on the working fluid in the new test system. Due to the undersized heat exchanger, the temperature of the working fluid in the new system gradually rose by 5°F throughout the course of the experiment. However, the discrepancy in volumetric efficiency is more largely affected by the fact that the initial starting temperature of the working fluid in the closed-loop system was higher than the previous system due to timing of the experiment and environmental effects. The new system was run in the summer while the old system was run in the winter. This caused a 25°F difference in initial starting temperature of the working fluid. Due to this temperature difference the viscosity of air increased by 4%, the viscosity of water reduced by 30%, and the density of the air reduced by 5%. Additionally, the temperature difference caused the dissimilar metals in the twin-screw pump to expand at different rates, affecting the screw clearances.

The volumetric efficiency of the pump at 50 psi inlet pressure is shown in Figure 40 and Figure 41. At 50 psi inlet pressure, the volumetric efficiencies using the two test facilities are more similar than in the 15 psi case. The maximum uncertainty found for the volumetric efficiency measurement is 1.11%, with the detailed analysis found in Appendix A. The main difference is that the previous facility recorded a faster rate of efficiency decline with respect to increasing differential pressure. This again is likely caused by temperature differences in the testing fluids, and can be reduced by incorporating a larger heat exchanger that is more easily able to regulate the working fluid temperature between summer and winter months.

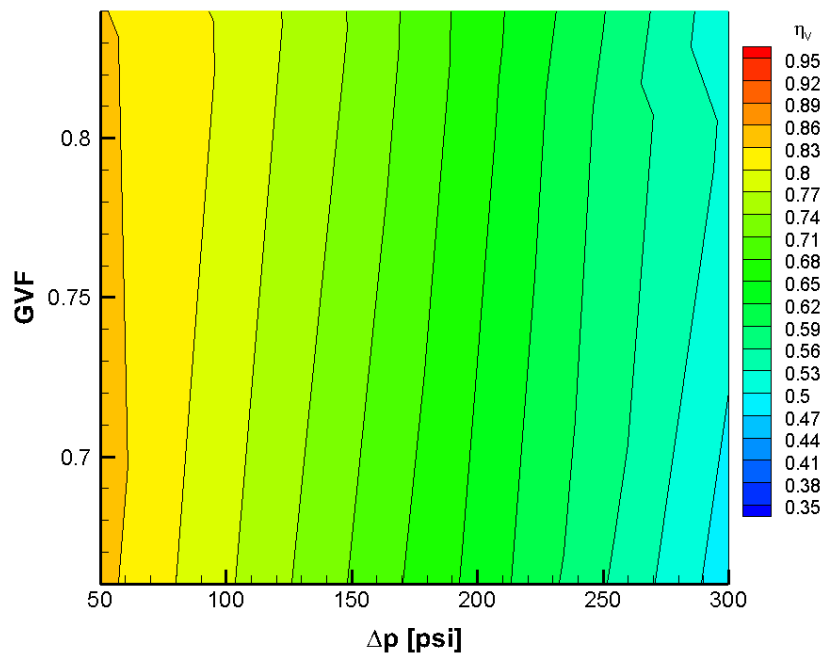


Figure 40: Volumetric efficiency in new facility (50 psi inlet, 900 RPM, 105°F)

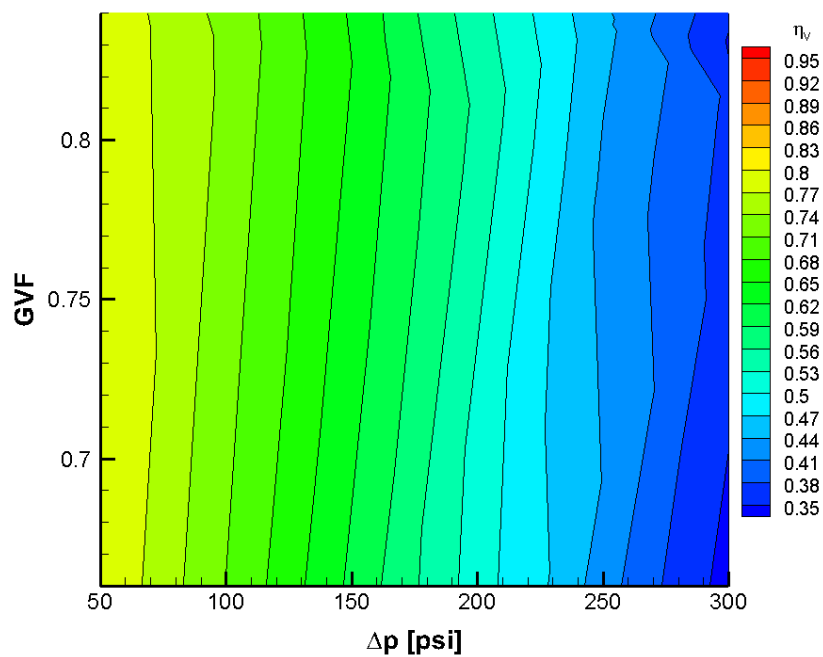


Figure 41: Volumetric efficiency in previous facility (50 psi inlet, 900 RPM, 75°F)

5.2.2 Mechanical Efficiency

The mechanical efficiency of the pump using the two different test systems is shown in Figure 42 and Figure 43. The mechanical efficiency of the pump is simply a ratio of the isothermal power imparted to the fluid to the electric power supplied by the pump. Since the new test facility recorded higher volumetric efficiency when compared with the previous facility, it follows that the mechanical efficiency is also higher in the new facility due to the increased volume of gas being compressed, and thus more power is transmitted to the gas with the same electric power. Again, this difference is most likely due to the temperature difference when testing in these two facilities. The uncertainty analysis of the mechanical efficiency at 15 psi inlet pressure yielded a maximum uncertainty of 1.91%. The detailed uncertainty analysis is found in Appendix A.

As expected, the mechanical efficiencies shown in Figure 42 and Figure 43 exhibit very similar behavior, and the new test facility recorded a slightly higher mechanical efficiency due to the difference in temperatures.

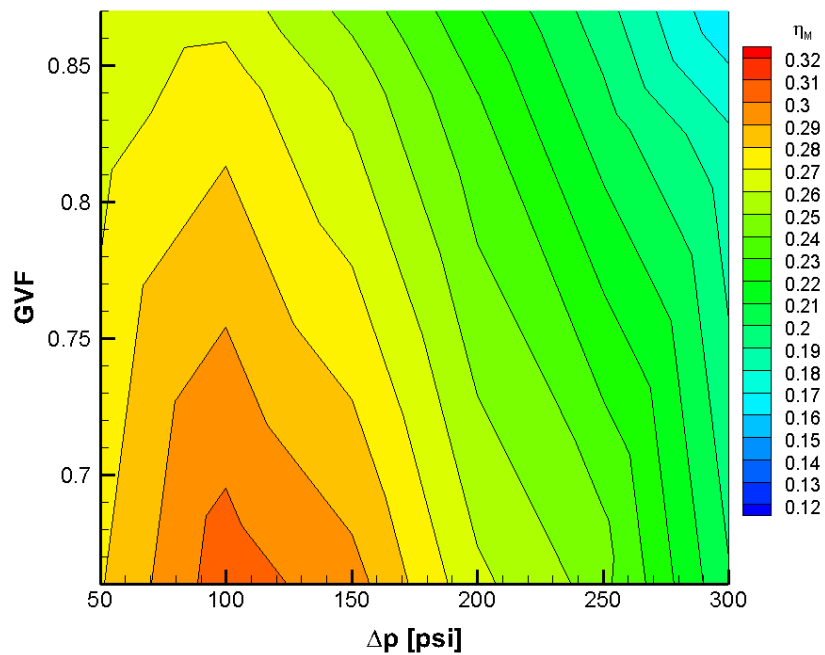


Figure 42: Mechanical efficiency in new facility (15 psi inlet, 900 RPM, 100°F)

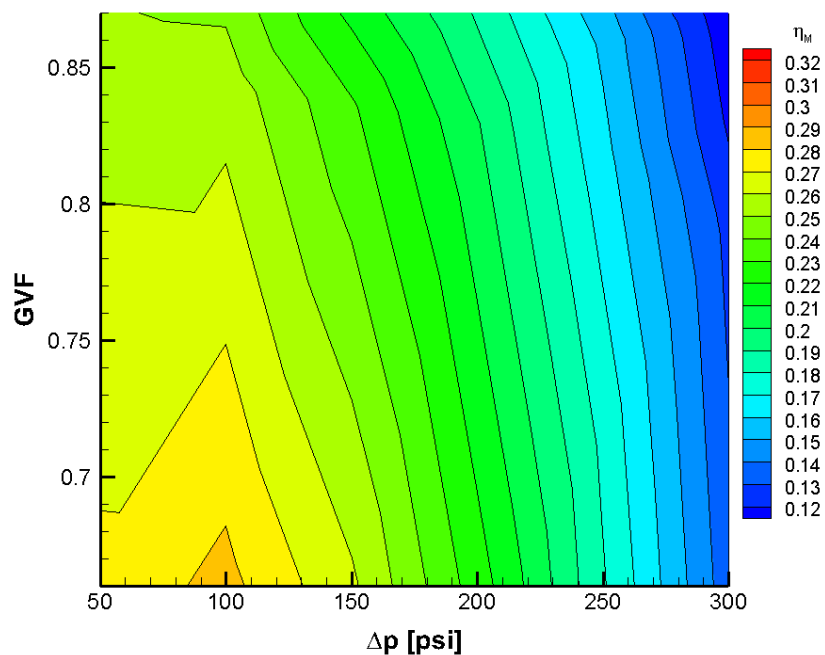


Figure 43: Mechanical efficiency in previous facility (15 psi inlet, 900 RPM, 75°F)

The mechanical efficiency of the pump at 50 psi inlet pressure is shown in Figure 44 and Figure 45.

The trend of mechanical efficiency at 50 psi is again very similar between the two test facilities. The new facility recorded a slightly higher mechanical efficiency while operating with an inlet pressure of 50 psi than was recorded in the previous test facility. A performance peak at 100psi differential pressure was observed at both 15 psi and 50 psi inlet pressures in the new test facility.

Additionally, it was observed that the difference in temperature of the working fluid affected the behavior of the peak performance of the mechanical efficiency. At the higher temperature of the new test facility, the peak was very well defined. In the previous facility, the cooler working fluid spread the lower-magnitude performance peak to lower differential pressures.

The maximum uncertainty of the mechanical efficiency measurement at 50 psi inlet pressure was found to be 1.65%. A detailed uncertainty analysis can be found in Appendix A.

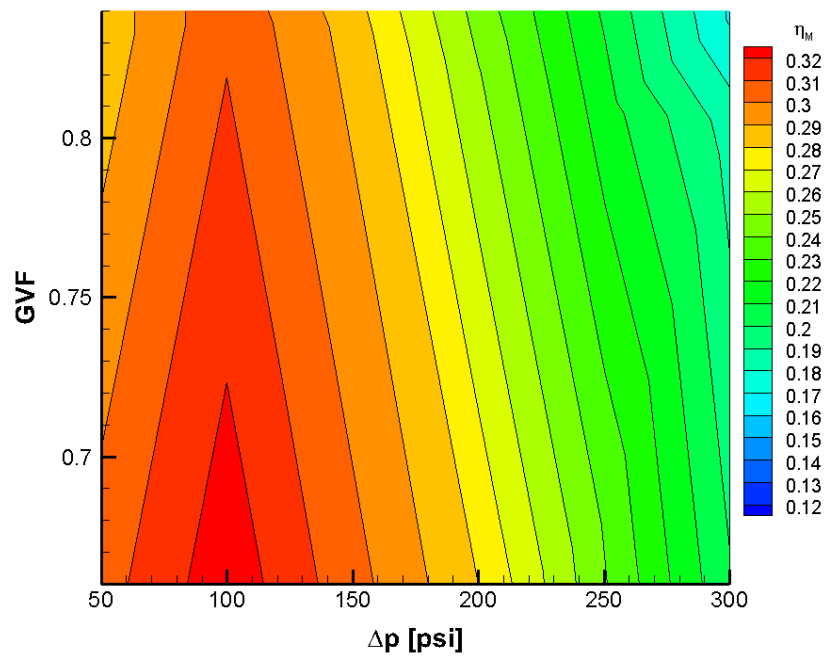


Figure 44: Mechanical efficiency in new facility (50 psi inlet, 900 RPM, 105°F)

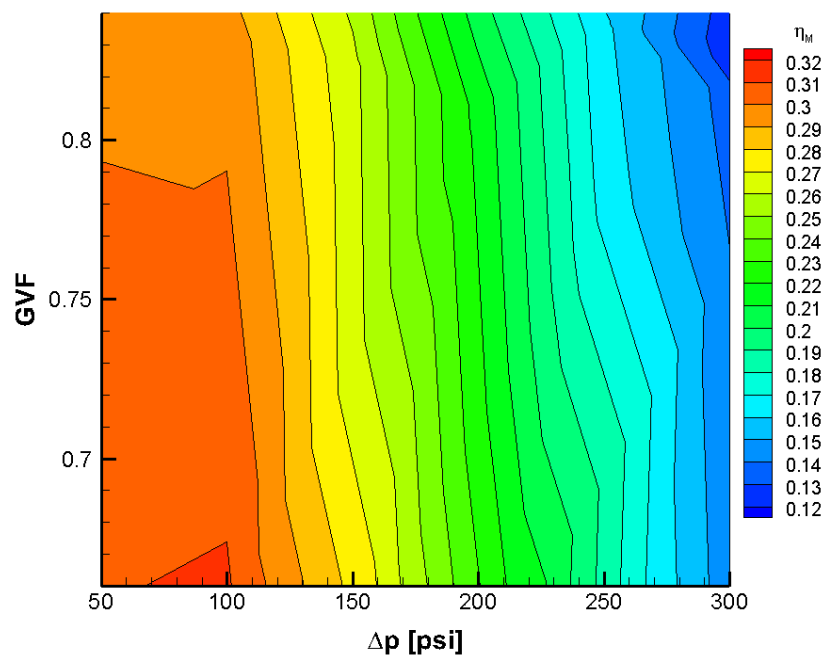


Figure 45: Mechanical efficiency in previous facility (50 psi inlet, 900 RPM, 75°F)

5.2.3 Effectiveness

The comparison of the effectiveness of the pump is shown in Figure 46 and Figure 47.

The effectiveness of the pump is the ratio of the actual power imparted to the liquid/gas mixture to the maximum power that would be imparted to a pure liquid. This parameter is based on thermodynamic principles, and should therefore not be affected by the geometry of the testing facility. However, some variation can be expected between the old and new facility due to the difference in the working fluid temperature discussed in previous sections.

As shown in Figure 46 and Figure 47, the pump effectiveness is extremely similar. This is to be expected because the thermodynamics do not appreciably change even with regard to temperature. The fact that the two test facilities exhibit similar effectiveness curves is evidence that the pressure transducers, temperature sensors, and flow meters were sufficiently calibrated to reproduce the results from the previous facility. The maximum uncertainty for the pump effectiveness at 15 psi inlet pressure was found to be 0.87%. A detailed analysis of this uncertainty can be found in Appendix A.

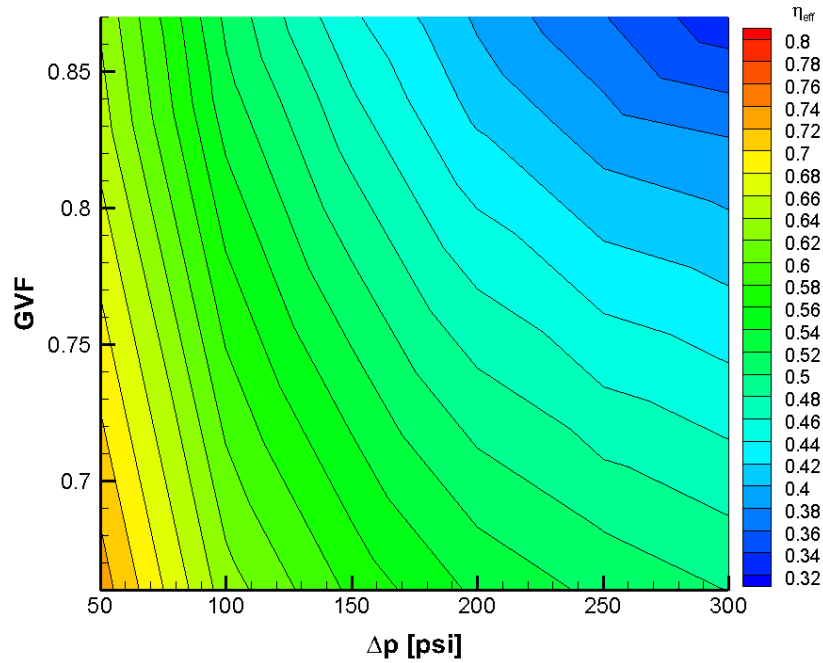


Figure 46: Pump effectiveness in new facility (15 psi inlet, 900 RPM, 100°F)

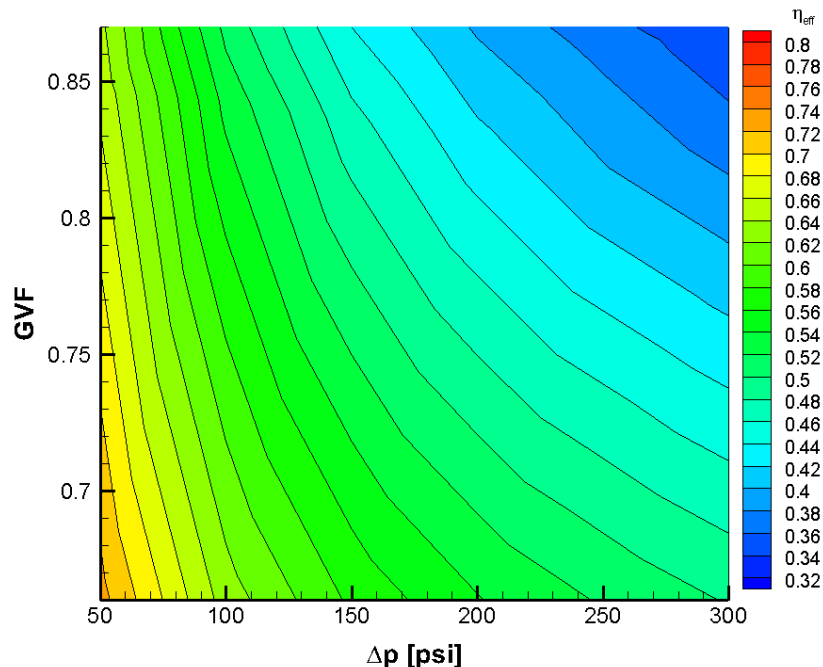


Figure 47: Pump effectiveness in previous facility (15 psi inlet, 900 RPM, 75°F)

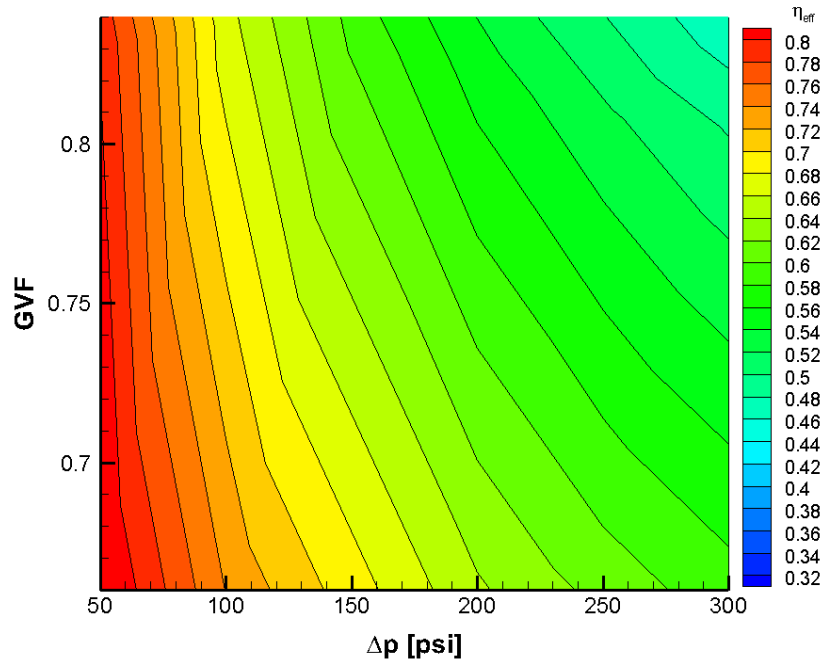


Figure 48: Pump effectiveness in new facility (50 psi inlet, 900 RPM, 105°F)

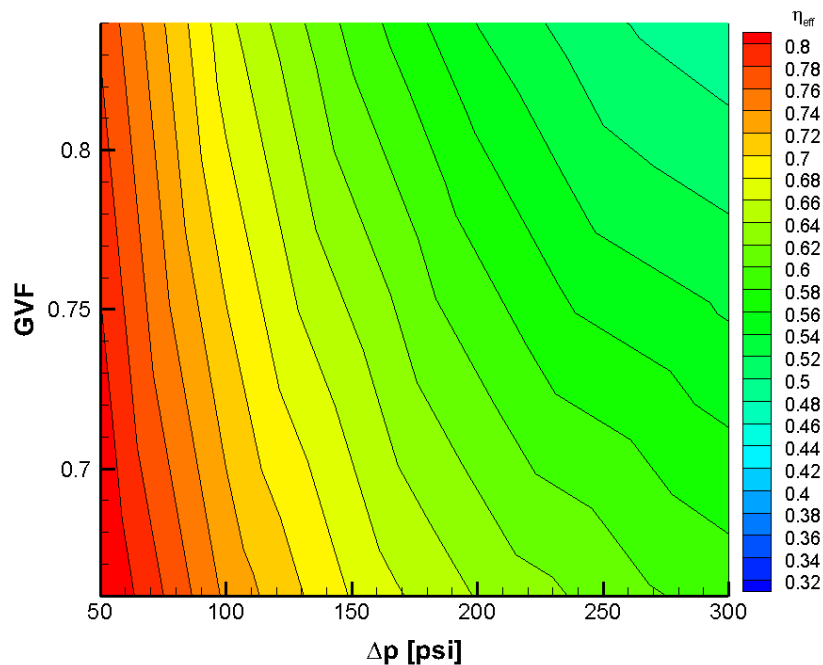


Figure 49: Pump effectiveness in previous facility (50 psi inlet, 900 RPM, 75°F)

As shown in Figure 48 and Figure 49, the pump effectiveness measured in the new facility continued to exhibit nearly identical characteristics to the pump effectiveness measured from the previous facility. This again suggests that the data acquisition equipment performed acceptably. The maximum uncertainty found for the pump effectiveness at 50 psi inlet pressure was determined to be 0.76%. This analysis can be found in Appendix A.

6 CONCLUSIONS

6.1 Conclusions

The new test facility was able to test the performance of a twin-screw pump and achieve results very comparable to the previous test facility. The new facility also has an advantage in that it can test at much higher inlet pressures than the previous test facility. The disadvantage of the new facility is that oscillating pressure response of the system in the inlet and outlet pressures must be addressed if true steady state testing is desired. The heat exchangers of the current facility were determined to be somewhat effective in moderating the temperature of the working fluid, but larger heat exchangers must be used if the pump will be run at full speed with this facility.

6.2 Recommendations

6.2.1 Air Valve

The air valve used in the air line between the separator and the pump inlet was oversized, and a smaller valve should be used for more exact flow control. The valve controller operates in the 4-20mA range, and does not fully close, even at 4mA. During testing, the highest signal sent to the valve was 5mA, meaning that even with the valve only slightly open, enough air was able to enter the system.

It is also recommended that the new system be designed in such a way that both the air and water valves can be open when starting up the system for ease of use. The current

pump's seal flush line had to be started before the pump was started. The seal flush would quickly fill up the pump inlet with water until it reached the air inlet line from the separator. The water would then continue to fill the air line. Even with the electro-pneumatic valve completely closed, some leakage occurred around the valve. In order to prevent the excessive amounts of water from damaging the turbine air flow meter and the air filters, a ball valve was used to manually close the air line during start up. However, the startup procedure still had to occur very quickly, because the air hose connecting the pump to the air valve could not withstand the pressure induced by the circulation pump, and would leak excessively if the pressure rose too high.

6.2.2 Oscillations

It is also recommended that further action be taken to reduce the oscillations observed in the pump inlet and outlet pressure. One possible solution involves lengthening the pump outlet pipe before the valve to damp outlet pulsations, or adding a diaphragm designed to absorb pulsations.

6.2.3 High Inlet Pressure

The test facility is currently limited in pressure to about 100 psi working pressure, due to hoses and 150 class piping used, as well as the plastic tubing used for the separator water level sight glass. If the low pressure water and air hoses, pipes, and flanges are replaced, the limiting factor will be the heat exchanger tubing, which is rated to 300 psi.

REFERENCES

- [1] Shippen, M., and Scott, S., 2002, "Multiphase Pumping as an Alternative to Conventional Separation, Pumping and Compression," Proceedings of the 34th Annual PSIG Meeting, Anonymous Portland, OR, pp. 2.
- [2] Cooper, P., Schiavello, B., de Marolles, C., 1996, "Tutorial on Multiphase Gas-Liquid Pumping," Proceedings of the Thirteenth International Pump User Symposium, Anonymous Texas A&M University, College Station, TX, pp. 159.
- [3] Kroupa, R., 2011, "Investigation of a Multiphase Twin-Screw Pump Operating at High Gas Volume Fractions," .
- [4] Vauth, T., and Reichwage, M., 2004, "Test Facility for Multiphase Pumps in Serial and Parallel Operation," Proceedings of the International Mechanical Engineering Congress Exposition, Anonymous American Society of Mechanical Engineers, pp. 449.
- [5] Egashira, K., Shoda, S., Tochikawa, T., 1998, "Backflow in Twin-Screw-Type Multiphase Pump," Old Production & Facilities, **13**(1) pp. 64-69.
- [6] Merah, N., Irfan-ul-Haq, M., and Khan, Z., 2003, "Temperature and Weld-Line Effects on Mechanical Properties of CPVC," Journal of Materials Processing Technology, **142**(1) pp. 247-255.

APPENDIX A

UNCERTAINTY ANALYSIS

A.1 Water Flow Rate

The equipment uncertainty is given in Table 7.

Table 7: Liquid flow rate measurement equipment uncertainty

Equipment Model	Measurement Range	Uncertainty	Symbol
Daniel Industries 1503-1D Flow Meter	22-225 GPM	$\pm 0.25\%$	$\mu_{k,WFM1}$
Omega FTB-1425 Flow Meter	5-50 GPM	$\pm 1.00\%$	$\mu_{k,WFM2}$
Omega FTB-1422 Flow Meter	0.75-7.5 GPM	$\pm 1.00\%$	$\mu_{k,WFM3}$
Omega FTB-1425 Flow Meter (seal flush)	5-50 GPM	$\pm 1.00\%$	$\mu_{k,seal}$
Omega iServer MicroServer	1Hz-100KHz	$\pm 0.30\%$	μ_f

A single water flow meter is used in parallel with the seal flush flow meter to provide the water flow rate for the system. Therefore, the equation for water flow rate is given by:

$$Q_{liq} = 60 \frac{f_{WFMn}}{k_{WFMn}} + 60 \frac{f_{seal}}{k_{seal}} \quad (13)$$

Where f_{WFMn} is the frequency output of the n th flow meter used, f_{seal} is the frequency output of the seal flush flow meter, k_{WFMn} is the k -value of the main flow meter used, and k_{seal} is the k -value of the seal flush flow meter.

Therefore the equation for the uncertainty in the water flow rate is given by:

$$\mu_{liq} = \left[\left(\frac{\partial Q_{liq}}{\partial f_{WFMn}} \mu_f \right)^2 + \left(\frac{\partial Q_{liq}}{\partial k_{WFMn}} \mu_{k,WFMn} \right)^2 + \left(\frac{\partial Q_{liq}}{\partial f_{seal}} \mu_f \right)^2 + \left(\frac{\partial Q_{liq}}{\partial k_{seal}} \mu_{k,seal} \right)^2 \right]^{1/2} \quad (14)$$

Simplifying:

$$\mu_{liq} = \left[\left(\frac{60}{k_{WFMn}} \mu_f \right)^2 + \left(-\frac{60f_{WFMn}}{k_{WFMn}^2} \mu_{k,WFM} \right)^2 + \left(\frac{60}{k_{seal}} \mu_f \right)^2 + \left(-\frac{60f_{seal}}{k_{seal}^2} \mu_{k,seal} \right)^2 \right]^{1/2} \quad (15)$$

Using the recorded k and f values that produce the largest uncertainty and taking into account the 16 GPM seal flush flow rate, the water flow rate uncertainties are listed in Table 8.

Table 8: Water flow meter uncertainties

Main Flow Meter Used	Total Water Flow Rate [GPM]	Total Uncertainty [%]	Total Uncertainty [GPM]
Daniel Industries 1503-1D Flow Meter	241.0	0.37%	0.894
	38.5	0.49%	0.189
Omega FTB-1425 Flow Meter	66.0	0.83%	0.548
	21.0	0.83%	0.175
Omega FTB-1422 Flow Meter	23.5	0.79%	0.184
	16.75	1.00%	0.167

A.2 Air Flow Rate

For air, the equipment uncertainty is given by Table 9.

Table 9: Air flow rate measurement equipment uncertainties

Equipment Model	Measurement Range	Uncertainty	Symbol
Daniel Industries 2 Inch Gas Turbine Meter	10-100 CFM	$\pm 1.00\%$	$\mu_{k,AFM}$
Omega iServer MicroServer	1Hz-100KHz	$\pm 0.30\%$	$\mu_{f,AFM}$
Omega TQSS- 116 T-type Thermocouple	32-662°F	$\pm 0.75\%$	μ_T
Omega PX481A Pressure Transducer	0-200 psi	$\pm 0.30\%$	μ_P
NI 9213 Thermocouple Input Module	± 78.125 mV	$\pm 0.30\%$	μ_{TM}
NI 9205 Analog Input Module	± 10 V	$\pm 0.062\%$	μ_{PM}

The equation for the volumetric flow rate of gas at the flow meter is given below:

$$Q_{AFM} = 60 \frac{f_{AFM}}{k_{AFM}} \quad (16)$$

The overall uncertainty for the volumetric flow rate at the flow meter is the sum of the flow meter uncertainty and the MicroServer uncertainty, given in the equation below.

$$\mu_{AFM} = \left[\left(\frac{\partial Q_{AFM}}{\partial f_{air}} \mu_{f,air} \right)^2 + \left(\frac{\partial Q_{AFM}}{\partial k_{air}} \mu_{k,air} \right)^2 \right]^{1/2} \quad (17)$$

Simplifying:

$$\mu_{AFM} = \left[\left(\frac{60}{k_{AFM}} \mu_{f,AFM} \right)^2 + \left(-\frac{60f_{AFM}}{k_{AFM}^2} \mu_{k,AFM} \right)^2 \right]^{1/2} \quad (18)$$

Using recorded frequency values that produce the largest uncertainty, the air flow meter uncertainties are calculated and listed in Table 10.

Table 10: Air flow meter uncertainties

Air Flow Rate	Total Flow Meter Uncertainty [%]	Total Flow Meter Uncertainty [CFM]
100 CFM	1.044%	1.044
10 CFM	1.044%	0.104

The equation for air flow rate at the pump inlet is more complex, given that the air valve throttling the flow is in between the flow meter and the pump inlet. Therefore the volumetric flow rate at the pump inlet must be calculated in terms of the volumetric flow rate at the flow meter. Using the ideal gas law and conservation of mass applied to point 1 (before the valve) and point 2 (after the valve), one can prove the following, where temperature and pressure are in absolute terms.

$$Q_2 = Q_1 \frac{p_1 T_2}{p_2 T_1} \quad (19)$$

Therefore the uncertainty of the volumetric flow rate of gas at the pump inlet is:

$$\mu_{gas} = \left[\left(\frac{\partial Q_2}{\partial T_1} \mu_{T1} \right)^2 + \left(\frac{\partial Q_2}{\partial T_2} \mu_{T2} \right)^2 + \left(\frac{\partial Q_2}{\partial p_1} \mu_{p1} \right)^2 + \left(\frac{\partial Q_2}{\partial p} \mu_{p2} \right)^2 + \left(\frac{\partial Q_2}{\partial Q_1} \mu_{Q1} \right)^2 \right]^{1/2} \quad (20)$$

Simplifying:

$$\mu_{gas} = \left[\left(-\frac{Q_1 T_2 p_1}{T_1^2 p_2} \mu_{T1} \right)^2 + \left(\frac{Q_1 p_1}{T_1 p_2} \mu_{T2} \right)^2 + \left(\frac{Q_1 T_2}{T_1 p_2} \mu_{p1} \right)^2 + \left(-\frac{Q_1 T_2 p_1}{T_1 p_2^2} \mu_{p2} \right)^2 + \left(\frac{T_2 p_1}{T_1 p_2} \mu_{Q1} \right)^2 \right]^{1/2} \quad (21)$$

Pressure and temperature values from the experimental data that would produce the largest percentage of error are used. Uncertainty values at inlet pressures of 15 psi and 50 psi are listed in Table 11.

Table 11: Air flow rate uncertainty at pump inlet

Pump Inlet Pressure	Air Flow Rate at Flow Meter [CFM]	Air Flow Rate at Pump Inlet [CFM]	Total Uncertainty at Pump Inlet [%]	Total Uncertainty at Pump Inlet [CFM]
15 psi	100	302.43	1.51%	4.57
	10	30.24	1.51%	0.45
50 psi	100	138.68	1.33%	1.84
	10	13.87	1.33%	0.18

A.3 Gas Volume Fraction:

The gas volume fraction of the working fluid is given by:

$$GVF = \frac{Q_{gas}}{Q_{liq} + Q_{gas}} \quad (22)$$

Therefore the uncertainty of the GVF calculation is given by:

$$\mu_{GVF} = \left[\left(\frac{\partial GVF}{\partial Q_{liq}} \mu_{Q_{liq}} \right)^2 + \left(\frac{\partial GVF}{\partial Q_{gas}} \mu_{Q_{gas}} \right)^2 \right]^{1/2} \quad (23)$$

Which simplifies to:

$$\mu_{GVF} = \left[\left(-\frac{Q_{gas}}{(Q_{liq} + Q_{gas})^2} \mu_{Q_{liq}} \right)^2 + \left(\frac{Q_{liq}}{(Q_{gas} + Q_{liq})^2} \mu_{Q_{gas}} \right)^2 \right]^{1/2} \quad (24)$$

Using the values at the extremes of the testing range, it is determined that the GVF has the uncertainties listed in Table 12.

Table 12: GVF uncertainty

Pump Inlet Pressure	GVF (with seal flush)	Air Flow Rate [GPM]	Water Flow Rate [GPM]	Total Uncertainty [% of GVF]	Total Uncertainty [GVF]
15 psi	0.91	261	25	0.15%	0.0014
	0.65	185	96	0.62%	0.0041
50 psi	0.91	233	24	0.15%	0.0013
	0.63	96	55	0.57%	0.0036

A.4 Volumetric Efficiency

The volumetric efficiency is given in the following equation, where Q_{th} is the theoretical volumetric flow rate, given by the pump geometry and pump speed:

$$\eta_V = \frac{Q_{liq} + Q_{gas}}{Q_{th}} \quad (25)$$

Therefore the uncertainty of the volumetric efficiency is:

$$\mu_{\eta_V} = \left[\left(\frac{\partial \eta_V}{\partial Q_{liq}} \mu_{Q_{liq}} \right)^2 + \left(\frac{\partial \eta_V}{\partial Q_{gas}} \mu_{Q_{gas}} \right)^2 \right]^{1/2} \quad (26)$$

Simplifying:

$$\mu_{\eta_V} = \left[\left(\frac{1}{Q_{th}} \mu_{Q_{liq}} \right)^2 + \left(\frac{1}{Q_{th}} \mu_{Q_{gas}} \right)^2 \right]^{1/2} \quad (27)$$

Substituting previously calculated values, the volumetric efficiency uncertainty is obtained in Table 13.

Table 13: Volumetric efficiency uncertainty

Pump Inlet Pressure	Water Flow Rate [GPM]	Air Flow Rate [GPM]	η_v	η_v Uncertainty [%]
15 psi	25	261	0.90	1.25%
	68	102	0.54	0.52%
50 psi	24	233	0.81	1.11%
	55	96	0.48	0.48%

A.5 Mechanical Efficiency

The mechanical efficiency of the pump is given by:

$$\eta_m = \frac{P_p}{P_e} \quad (28)$$

Substituting the analytical equations for net power imparted to the fluid and the electric power of the pump:

$$\eta_m = \frac{Q_{liq}(p_2 - p_1) + p_1 Q_{gas} \ln\left(\frac{p_2}{p_1}\right)}{V_{ml}} \quad (29)$$

Substituting into the Kline-McClintock uncertainty analysis equation:

$$\mu_{\eta m} = \left[\left(\frac{\partial \eta_m}{\partial Q_{liq}} \mu_{Q_{liq}} \right)^2 + \left(\frac{\partial \eta_m}{\partial Q_{gas}} \mu_{Q_{gas}} \right)^2 + \left(\frac{\partial \eta_m}{\partial p_1} \mu_{p1} \right)^2 + \left(\frac{\partial \eta_m}{\partial p_2} \mu_{p2} \right)^2 + \left(\frac{\partial \eta_m}{\partial V_{ml}} \mu_{V_{ml}} \right)^2 \right]^{1/2} \quad (30)$$

Using uncertainty values previously obtained, the final uncertainty values for the mechanical efficiency are given in Table 14. The extreme cases of low differential pressure/low GVF and high differential pressure/high GVF were used for each inlet pressure.

Table 14: Mechanical efficiency uncertainty

Pump Inlet Pressure	Water Flow Rate [GPM]	Air Flow Rate [GPM]	η_m	η_m Uncertainty [%]
15 psi	22.0	192.3	0.15	1.19%
	96.8	185.7	0.26	1.91%
50 psi	20.4	142.6	0.17	1.06%
	91.1	175.4	0.31	1.65%

A.6 Pump Effectiveness

The pump effectiveness is given by the following equation:

$$\eta_{eff} = \frac{P_p}{P_h} \quad (31)$$

Substituting the definition of the net isothermal pump power and the hydraulic pressure previously given in Section 2.2, the effectiveness becomes:

$$\eta_{eff} = \frac{Q_{liq}\Delta p + p_1 Q_{gas} \ln\left(\frac{p_2}{p_1}\right)}{(Q_{liq} + Q_{gas})\Delta p} \quad (32)$$

Therefore the uncertainty of the effectiveness is:

$$\mu_{\eta_{eff}} = \left[\left(\frac{\partial \eta_{eff}}{\partial Q_{liq}} \mu_{Q_{liq}} \right)^2 + \left(\frac{\partial \eta_{eff}}{\partial Q_{gas}} \mu_{Q_{gas}} \right)^2 + \left(\frac{\partial \eta_{eff}}{\partial p_1} \mu_{p1} \right)^2 + \left(\frac{\partial \eta_{eff}}{\partial p_2} \mu_{p2} \right)^2 \right]^{1/2} \quad (33)$$

Substituting previously calculated values and simplifying, the pump effectiveness uncertainty is determined. The pump effectiveness uncertainty is listed in Table 15.

Table 15: Pump effectiveness uncertainty

Pump Inlet Pressure	Water Flow Rate [GPM]	Air Flow Rate [GPM]	η_{eff}	η_{eff} Uncertainty [%]
15 psi	22.0	192.3	0.31	0.75%
	96.8	185.7	0.76	0.87%
50 psi	20.4	142.6	0.45	0.57%
	91.1	175.4	0.83	0.76%